Experimental and Numerical Study of Parametric Dependence of Lift in Flapping Flight

A Thesis

Submitted for the degree of

Master of Science (Engineering)

By

Devranjan Samanta

Engineering Mechanics Unit
Jawaharlal Nehru Centre for Advanced Scientific Research
Bangalore -560064

Dedicated to my parents

DECLARATION

I hereby declare that the matter embodied in the thesis entitled "**Experimental and Numerical Study of Parametric Dependence of Lift in Flapping Flight**" is the results of the investigations carried out by me at the Engineering Mechanics Unit (EMU), Jawaharlal Nehru Centre for Advanced Scientific Research, Bangalore under the supervision of Prof. K R Sreenivas and that it has not been submitted elsewhere for the award of any degree or diploma.

In keeping with the general practice in reporting scientific observations, due acknowledgment has been made whenever the work is described based on the findings of other investigators.

_____

Devranjan Samanta

CERTIFICATE

I hereby certify that the matter embodied in the thesis entitled **"Experimental and Numerical Study of Parametric Dependence of Lift in Flapping Flight"** has been carried out by Mr.Devranjan Samanta at Engineering Mechanics Unit, Jawaharlal Nehru centre for Advanced Scientific Research, Bangalore, India under my supervision and that it has not been submitted elsewhere for the award of any degree or diploma.

_____

Prof. K. R. Sreenivas
(Research Supervisor)

CONTENTS

Acknowledgement

I am thankful to my parents for encouraging me during higher studies. Throughout the two years they took lot of pains so that I can study unperturbed.

Secondly, I am grateful to my advisor Prof. K R Sreenivas for his insightful suggestions. His gentle and patient approach helped me a lot in the initial days of my Masters programme. Also I am thankful to Prof Govardhan (IISc Mech), Prof Rama Govindarajan (JNCASR), Prof O N Ramesh and Prof Venkatraman (IISc Aerospace) for their splendid lectures on subjects related to fluid mechanics.

The acknowledgement list will be incomplete without mentioning my two B.Tech friends Bishakh and Soumik who motivated me to pursue higher studies.

Reaching JNC, I found my batch mate Anubhab to be extremely helpful regarding academic problems and also giving me a great company outside academic spheres. I am also thankful to my labmates Mukund, Rajapandyan, Vivek, Dhiraj and Dinesh for their cooperation and each of their association has been uniquely enjoyable in their own way. I am also thankful to Ashish, Ratul, Harish, Sumesh, Vivekanand and other members of our department for their enjoyable company.

Outside the department during playing table tennis I had great time with Dhiraj, Monojit, Kalyan, Leela, KKR dutta, Venki, KP, Abhisek only to name a few.

Last but not the least life in weekends would have been quite dull without my IISc friends Baidurya, Ishita, Wrichik, Arnab, Deboshruti, Preeta and Anupama. I am thankful to all of them.

List of Figures:

Abstract

Flapping wings exhibit better performance than the fixed wings as the size of the flying objects decrease. In nature flight by the flapping wings is predominant in case of insects and small birds. Motivated by this aspect engineers have been trying to devise Micro Air Vehicles (MAV) using flapping wings. Many interesting phenomena like delayed stall, leading edge vortex, wake capture etc., have been suggested as mechanism of lift generation & enhancers in the case of insect flapping flight. Our focus is on impact of asymmetry in upstroke speed and downstroke speed in lift generation and parametric study to find the optimum wing kinematics. Both experimental study using mechanical models and numerical simulations by using the Discrete Vortex Method (DVM) have been done to find the efficacy of this mechanism in lift generation. Influence of kinematic parameters like inclination of the mean position of the wings, amplitude and asymmetry ratio have been studied through numerical simulations. A brief study have been done to explore the impact of flexibility on lift generation through simulations.

In chapter 1, a brief overview of the previous works on the insect flight is discussed. Different unsteady mechanisms responsible for lift generation are briefly highlighted. In second chapter experimental evidence have been presented to show the effectiveness of asymmetric flapping over the symmetric flapping and influence of inclination of the mean position of the wings. In third chapter we present numerical simulations of flapping flight using 2-D discrete vortex method. Results of parametric dependence on lift are presented in the last chapter.

CHAPTER 1

INTRODUCTION

Insect flight has been an enigmatic phenomenon for long time. From biologists point of view it provides an insight into insect physiology and evolutionary process. For physicists and engineers insect flight performance at low Reynolds number is fascinating. Flapping mechanism of insects involves several interesting processes like leading edge vortex, delayed stall etc. It has been observed that the fixed wing airfoils don't exhibit a good performance in the regime of Reynolds number below 500000 (McMaster & Henderson 1980, Lissaman 1983, Mueller 1985) because of laminar boundary layer separation.

It has been envisaged by engineers that extensive study of the flapping mechanism within the low Reynolds number regime of 10-10000 would provide the clues for the optimum lift generation. One of the main motivations for the study of flapping flight is its applicability in the design of MAVs (micro air vehicle). These vehicles are useful in various types of applications including surveillance, communication relay links, ship decoy and detection of hazardous biological, chemical or nuclear spills. Although there is no strict definition of micro air vehicles, they are generally defined to have sizes of 15cm or 6 in) with a mass of 80 gram (Mueller & Delaurier 2003). One of the advantages of flapping mechanism is that at small sizes it generates lift and thrust without excessive weight (Delaurier & Harris 1982, Kellog et al (2001b). It may also utilize coupling between the flexible wings and aerodynamic forces (i.e. aeroelasticity) so as to improve aerodynamic performance.

Study of the insect flights is a challenge due to its small size and high flapping frequency. Separating aerodynamic forces from the inertial forces in free flight conditions has been a very tricky issue (Zanker and Gotz 1990). Also insects rely on visual feedback, so it's necess-

ary to check whether the lighting conditions do not change insect's behaviour (Sane 2003). However in recent times high speed photography have helped to determine the evolution of the flow field around the insect wings and has helped to gain insight into phenomena like flow separation & leading edge vortex stabilization (Ellington 1999). A lot of study has also been done using dynamically scaled mechanical models and using computational models for studying flapping flight. In this chapter we describe past literature with the major breakthroughs in analyzing the flapping mechanism of insects.

1.1 Unsteady aerodynamic features of insect flight:

a. Wagner effect : In 1925 Wagner has first proposed that an impulsively started wing from rest takes time in attaining the steady state circulations which is experimentally proved by Walker (1931). There may be two reasons, firstly there may be delay in attainment of the Kutta condition due to viscous action. Secondly the counteracting interaction of the shedded vortices on the bound circulation of the wing may be the cause of the delay. However Dickinson (1999), Walker (2002) have shown that Wagner effect is not effective in the Reynolds number regime 10-1000 relevant to the insects.

b. Clap and fling mechanism :

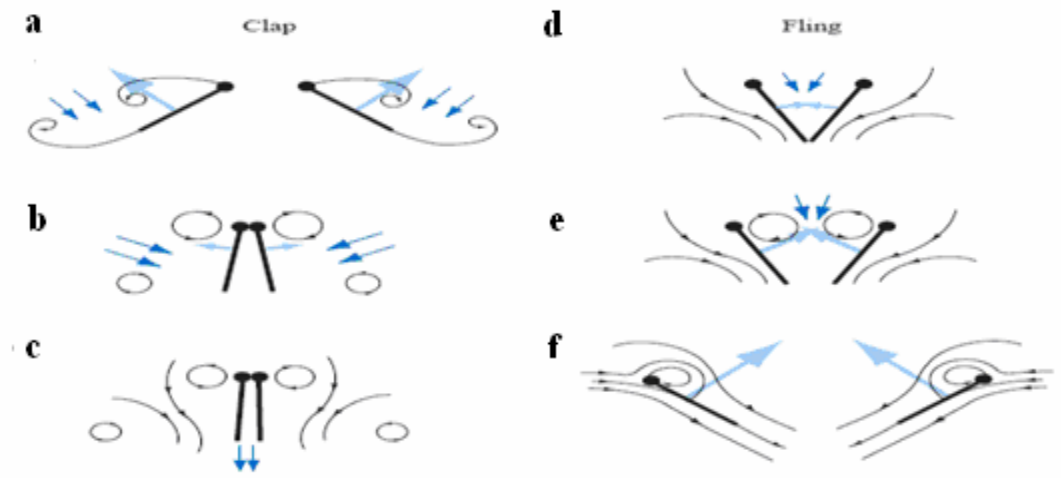

Figure1.1: Different stages of clap and fling mechanism (S.P. Sane 2003)

The clap and fling mechanism have been extensively studied by Weis-Fogh (1973), Lighthill (1973), Spedding and Maxworthy (1986). Figure 1.1 (a, b, c) constitutes clap process. Figure 1.1 (a, b) shows that the wings progressively closes starting from the leading edge. Figure 1.1 c shows that circulation of opposite nature of the wing nullifies each other thereby decreasing the shedded vortices. It prevents the Wagner effect and help in rapid growth of the circulation and utilization of the lift for greater period of the stroke. Moreover, jets emanated from the clapping wings provide lift in upward direction. Figure 1.1 d-f represents the fling mechanism. The leading edge continues to fling apart keeping the trailing edges stationary. In the low pressure region between wings fluid rushes in and helps in growth of circulation of opposite nature in the wings. The net circulation around two wings is zero there by obeying Kelvin's circulation theorem. However, Dickinson (1999) argues that the clap mechanism is not suitable as it results in substantial wear and damages. Although, he agrees that the fling can be used by the micro robots like tiny insects he opines that extra lift can be used by using higher wing beat frequency and relatively larger wings.

c. Delayed Stall:

Other interesting feature of the insect flight is their capacity to operate at higher angle of attack without any stall. As the insect wings are generally like rigid flat plates, at high angles of attack flow separates at the leading edge and then reattaches along the chord. So flow continues smoothly over the trailing edge. The leading edge separation zone is called leading edge bubble. This phenomena is called thin airfoil separation bubble. As stall occurs in this case later than conventional airfoils it's called delayed stall. Experimental evidence for this has been shown by Maxworthy (1979), Ellington (1979) and Dickinson et al (1999). Enhancement of lift due to the leading edge bubble have been proposed by Polhamus(1971). A schematic view of leading edge bubble

has been given in Fig 1.2 (a, b).

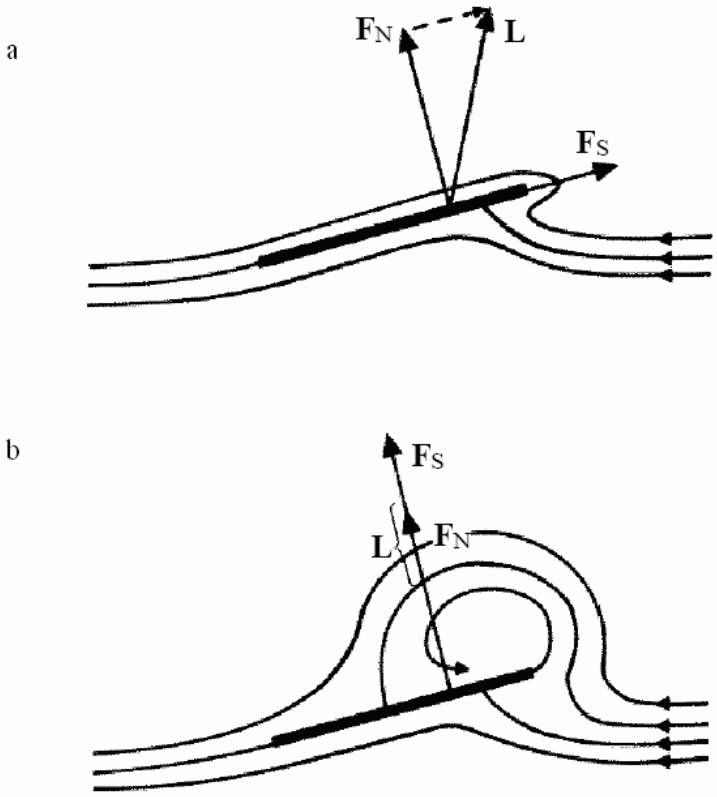

Fig **1.2** The generation of detached vortex lift by rotation of leading edge suction vector on thin wings. (a) Conventional steady-state lift results from potential flow around a wing section and the Kutta condition on the trailing edge. The rapid change in velocity around a sharp leading edge results in a suction vector ($\mathbf{F}_S$) that acts parallel to the chord and sums with the normal force ($\mathbf{F}_N$) to produce the total lift (**L**). (b) With the development of a leading edge vortex, a 'Kutta-like' condition replaces the rapid change in velocity around the leading edge, eliminating the parallel suction force. However, a suction force is now required to maintain the new attachment site on the upper surface, which adds directly with the normal force to generate a large increase in total lift. Thus, the change in pressure distribution resulting from the leading edge vortex is analogous to a 90° rotation of the leading edge suction vector.
(Dickinson 1993)

In Fig 1.3 the flow field due to leading edged bubble is shown. In their experiment of model hovering hawkmoths Dickinson et al (1999) show that a span wise steady flow occurs from wing hinge towards the wing tip, stabilizing the leading edge separation bubble. As this flow redirects the momentum in spanwise direction, momentum of the flow from along the chord-wise direction decreases resulting in a smaller leading edge vortex which can sustain the re-

attachment for a longer time. For the low aspect ratio (LAR) wings below ~ 1.5 these tip vortices are present over a greater area and therefore exerts a greater influence on its aerodynamic characteristics. These types of wings are assumed to have two sources of lift: (a) linear and (b) nonlinear. The linear lift is general lift due to circulation around airfoil. The non linear lift is created by the tip vortices form the low pressure cells on the wing's top surface, as is observed in delta wings at high angle of attack. This non linear effect increases the lift-curve slope as the angle of attack enhances, and it is considered to be responsible for the high value of stall angle (Delaurier 2003).

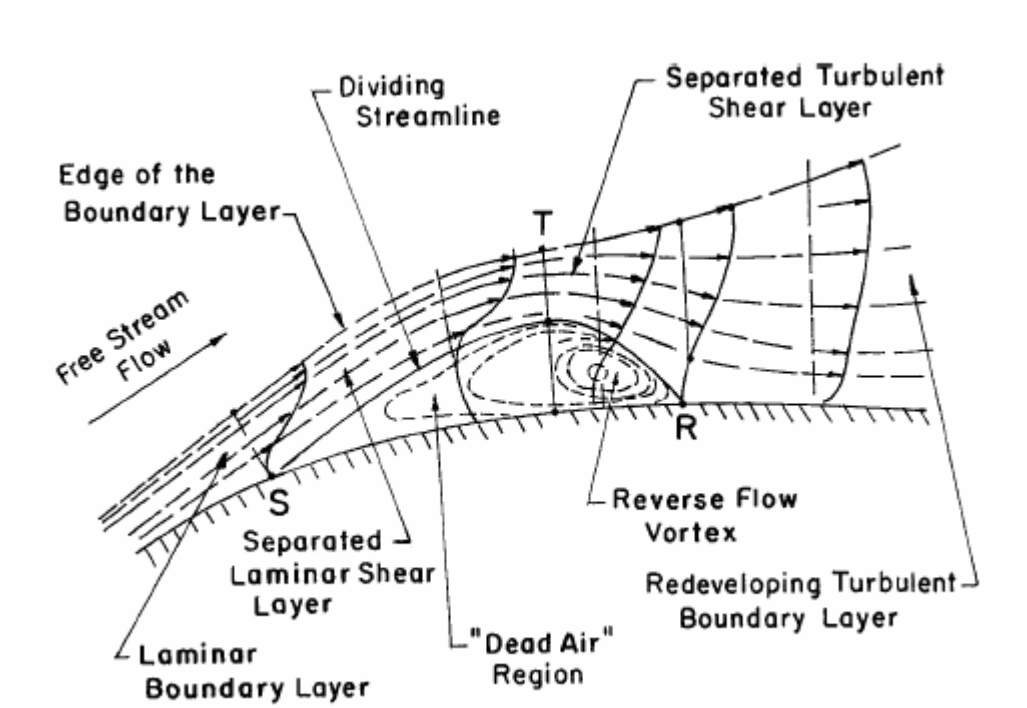

Fig 1.3 Time-averaged features of a transitional separation bubble (Horton 1968)

d. Kramer effect

At the end of each stroke, insect wings undergo substantial pronation and supination (rotation) about a spanwise axis (Dickinson et al,1993). During translation wings tend to rotate about the spanwise axis causing deviation from the Kutta condition and the stagnation point moves away

from the trailing edge. This results in a sharp velocity gradient at trailing edge. However due to viscous effect there is always a tendency to maintain the Kutta condition by generating additional circulation. With increasing angular speed Kutta condition may never be achieved but the tendency to achieve it creates additional circulation. In the context of aerodynamic flutter Kramer first noticed it in 1932 and it is so called Kramer effect. Alternatively it is termed as rotational lift by Dickinson (2002).

e. Added mass

Apart from the circulation based lift, there is a lift imparted by the surrounding fluid subjected to acceleration by the wings. Experimentally it's difficult to separate this effect from circulation based lift. Typically this effect is called added mass (Vogel 1994) or virtual mass (Ellington (1984 b) effect. It has been observed by Hamdani & Sun (2000) that the added mass forces are closely tied to the initial stages of flow separation and fluid acceleration.

f. Quasi steady modeling:

Studying flapping motion would have been easier if quasi steady modeling was sufficient for explaining the lift produced. The idea behind the modeling is to assume that the instantaneous aerodynamic forces on flapping wings are equal to forces during steady motion of the flapping wings at the identical instantaneous velocity and the angle of attack (Jensen 1956). However Ellington (1984a) showed that the mean lift during hovering is more than that predicted by the quasi steady model. Inadequacy of the model is further proved by Ennos (1989), Zanker Gotz (1990) and Dudley (1991).

g. Asymmetry in upstroke speed and downstroke speed

It has been shown by Shreyas (2005) through experiments and numerical simulation that lift is generated due to the asymmetry (difference) in the upstroke speed and downstroke speed.

Keeping parity with nature he imposed faster downstroke speed and showed that lift is produced. On the other hand the net lift over a cycle is nil for a symmetric flapping. In the symetric flapping he has shown that jets are emanated in four directions of the flow field implying equal momentum transfer in both upward and downward directions. Hence the net lift imparted to the wings over a cycle is nearly zero. However in asymmetric flapping two jets are emanated in downward direction. So the net upward momentum transferred to the wings generates an upward lift. Figure 1.4 a, b presents the flow structures due to symmetric and asymmetric flapping respectively.

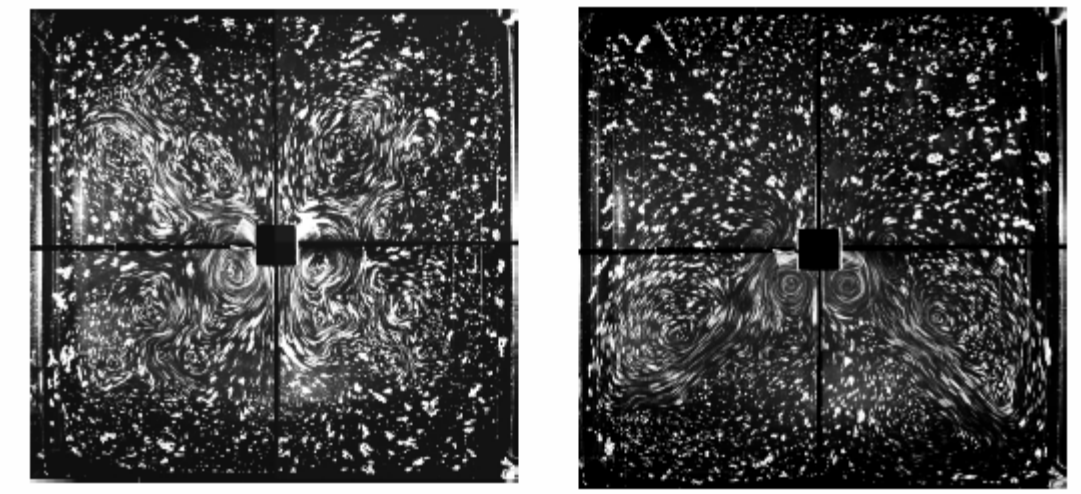

(a) **(b)**

Fig 1.4 (a) Symmetric flapping t_d=t_u=10 sec (b) asymmetric flapping t_d=10 sec, t_u =20 sec (Shreyash, 2005)

1.2 Physical Modeling of insect flight

Due to the difficulties in visualizing and analyzing the insect flights scientists have adopted dynamic scaling method to construct mechanical models. In order to preserve the fluid flow dynamic similarity, two parameters Reynolds number and reduced frequency parameter i.e. body velocity/wing velocity have to be similar for an insect and its model. Several unsteady

mechanisms like clap and fling (Bennet 1977; Maxworthy,1979; Spedding & Maxworthy 1986), delayed stall (Dickinson, Gotz 1993), rotational lift (Dickinson et al 1999; Sane & Dickinson 2002) and wing-wake interactions (Dickinson 1994; Dickinson et al 1999) have been studied in detail using this method.

1.3 Motivation and definition of the problem

The main factors that motivate us to study flapping mechanism are:

a) Wind tunnel testing of insect flights reveals that the measured forces are less than that essential for active flight (Ellington 1984). Quasi steady aerodynamic theory fails to predict the lift generated due to flapping flight.

b) Although many unsteady mechanisms have been identified for the lift generation, there is lack of engineering principles for optimum lift performance of MAVs. For optimum flight of MAVs there are different parameters like angular amplitude θ, inclination of the axis of mean position Φ, angular frequency ω, asymmetry ratio (upstroke frequency **:** downstroke frequency) size which affect the flight performance. Investigating the perfect regimes of these parameters for optimum flight performance have not been done earlier and demands attention. Figure 1.5 shows the mean position of the wing and angular amplitude.

c) Coupling of the aerodynamic forces with the wing flexibility is an interesting phenomena. Whether flexibility improves lift and finding out the optimal distribution on of the flexural rigidity along the wing is an interesting problem to study.

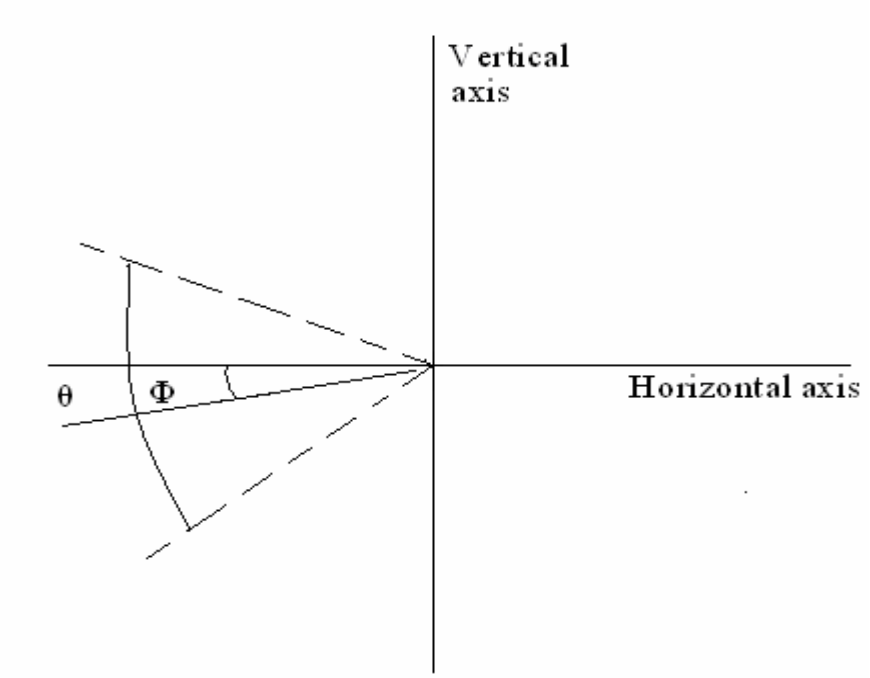

Fig 1.5 Φ: mean position of the wing, θ: angular amplitude of the wing

In this work we have tried to study simple mechanisms of lift generation in the regime of the Reynolds number around 1000. Also we have explored the parametric dependence of flapping flight. Impact of flexibility on flight performance has also been studied. We have carried out numerical simulation using 2-D discrete vortex method and experiments using mechanical flapping models.

CHAPTER 2
Experiments using mechanical models

With the increase in computational speed computer simulation of flapping flight has helped in understanding different mechanisms. Still, experimental studies are important in getting insights in understanding unsteady mechanisms of insect flight and in validating numerical simulations. Due to small size of the insect wings it's hard to place sensors and measure lift produced during each instant of flight. Even with high speed photography, it is difficult to do flow visualizations due to small size and making insects to fly in predefined and desired path. Considering these constraints, we have carried out the flow visualizations using mechanical flapping models based on dynamic similarity criterion (Reynolds number). In this set of experiments we have considered hovering flight configuration as the power required for this is maximum (Ennos 1989, Ellington 1984).

2.1 Experimental setup

We conducted the flow visualization experiments in a square tank with 1.2×1.2 square meter cross section and with a depth of 0.8 meters using water as working fluid. Flow visualization experiments are done around Re 1000, with wings of larger size ($50\text{cm} \times 8\text{cm}$) flapping at lower frequency. These wings are fitted to the steel rods and driven by a stepper motor which is further controlled by Galil motion controller card equipped with a resolution of 2 lakh counts per revolution.

Design and construction: Following are the components of experimental setup indicated in Fig 2.1.

1. Two rectangular wings of Perspex-sheet ($50\text{cm} \times 8\text{cm}$).

2. Two stainless steel rods are used as shafts on which wings are mounted.

3. A stepper motor housing.

4. Four hardened MS rods as harnesses for the wing shafts and the motor housing.

5. A brass base weighing 2 kg to hold the wing shafts in position at bottom of the tank.

6. Two halogen lamps, each of 300 watt power.

7. A vertical stand for mounting the camera. Pictures were taken from a position so that the camera's focal plane is parallel to the water surface.

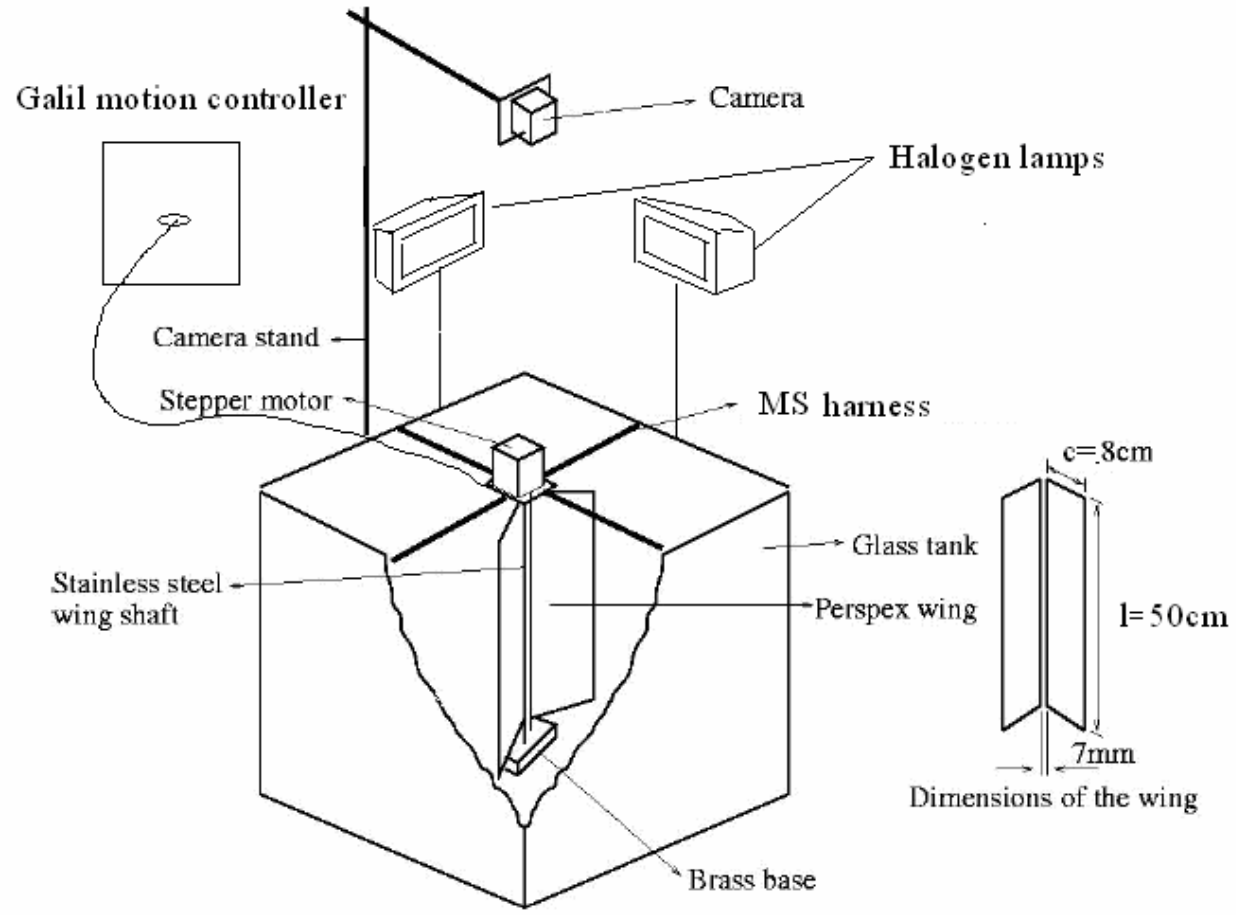

Fig 2.1 Schematic of the experimental setup

Design considerations of the wing:

In order to perform the flow visualization experiments we have to take care of certain design

considerations of the wing. The wing chord length c is used in experiments is 8cm except in two experiments where c is 14 cm. In order to satisfy the open boundary condition, the ratio of wing length to tank dimension should be large enough so that flow field is not affected by the presence of wall boundaries. Also the chord length should be large enough to do proper flow visualization. To reduce the three dimensional effects, aspect ratio (l/c) must be made as large as possible within practical limits. The wing aspect ratio (l/c) used is 6.25. Wing thickness is kept 3 mm, and gap between two rods is kept 7mm. Two wing shafts are coupled by two pairs of plastic gears whose pitch diameter was 13mm and wing shafts are of 6mm diameter.

Wing Kinematics

Flapping mechanism is driven so that wing angular velocity is a sinusoidal motion profile. The angular velocity is given as $\omega = \frac{\theta}{2} 2\pi f \sin(2\pi ft)$

where ω= angular velocity (radians/second), θ = angular amplitude (radians),

f= frequency (Hertz) and t= time (seconds).

Experiments have been used with two types of velocity profiles, symmetric and asymmetric flapping. In figure 2.2, the two velocity profiles are illustrated.

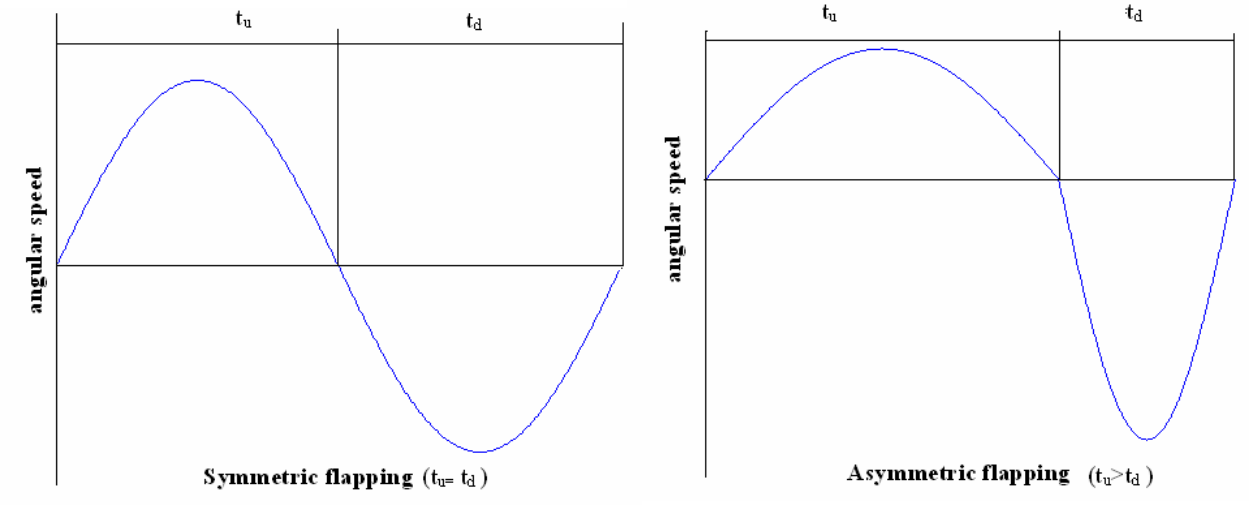

Figure 2.2 Variation of angular speed vs. time in symmetric and asymmetric flapping

Symmetric Flapping: In this type of flapping the upstroke period is equal to downstroke period (t_u=t_d).

Asymmetric flapping: In this type of flapping the downstroke time is less than the upstroke time (t_u>t_d). The asymmetry ratio (AR= t_d/ t_u) is an indication of degree of asymmetry. Shreyas (2005) has found that asymmetric flapping can produce lift. It is found in nature that birds and insects flap faster in the downstroke period compared to upstroke speed (Ennos1989). However, it is not known for a given situation what asymmetry ratio can produce maximum lift. The wings flap with θ amplitude about a mean position. The motion can be programmed through Galil software. In this motion Reynolds number is defined as**:**

$$\mathrm{Re} = \frac{\theta(2\pi f)\sin(2\pi ft)c^2}{2\nu}$$

2.2 Flow visualization Technique

In order to understand mechanism of lift generation in flapping flight our first attempt was to get some qualitative dependence observing the flow field. The unsteady flow field generated by flapping motion, is captured using a digital camera over a long exposure time (2-4 sec) to get an insight into the phenomena. For the flow visualization streak photography technique is used.

Streak Photography

Streak photography is a technique where long exposure pictures are taken of the dispersed particles in the fluid. The picture represents the pathline of the particle over that time. If the particles in flow field can faithfully follow the fluid motion, overall image of the pathlines of particles represents a vivid picture of the flow structure. For this purpose we used aluminium particles of 10 micron size sprinkled over the water. Two halogen lamps of 300 watt are used for illumination. A Canon camera whose settings can be remotely assigned by the

computer is used for taking pictures with a given exposure time. Exposure time is given 2 to 4 sec depending on the flapping frequency.

2.3 Results:

2.3.1 Symmetric flapping with Φ=0:

Starting with the mean position of the wings at zero degree (horizontal position) we drive the wings with an angular amplitude of 120^o i.e. 60^o on each side of the mean position. Figure 2.3 shows the configuration of the wing and velocity profile. Photographs have been taken at an interval of 7 seconds to capture the flow field at the end of downstroke, upstroke and at mean position. When the wings are at mean position Fig 2.4 c there are four jets in the four quadrants of the tank. Jets emanate from the centre and rush to four corners of tank. As momentum associated with jets in the upward direction and downward direction is almost equal in magnitude, so the lift averaged over a cycle is nearly zero.

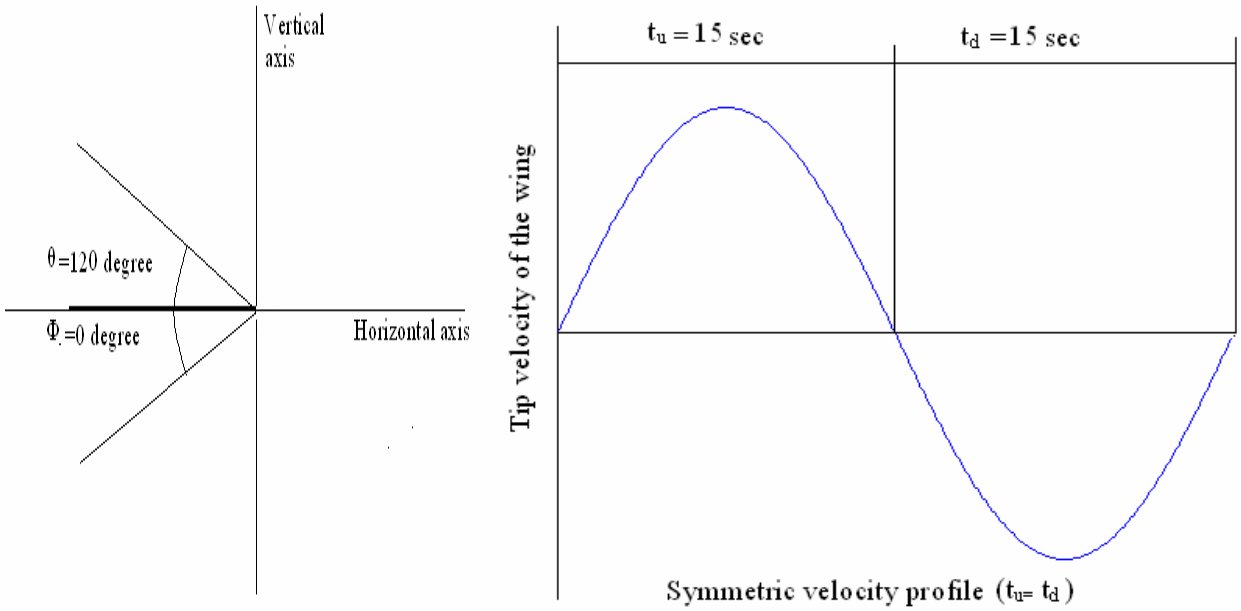

(a) **(b)**

Figure 2.3(a) wing configuration and its (b) symmetric velocity profile

Figure 2.4 a and b are the flow structures at end of upstroke and downstroke. The wakes seem to be moving downward with the downstroke speed. In the figures 2.4 a and b the wakes app-

ear to exchange their position. It can be argued that the upward momentum is nearly equal to downward momentum. So the net momentum over a cycle is nearly zero.

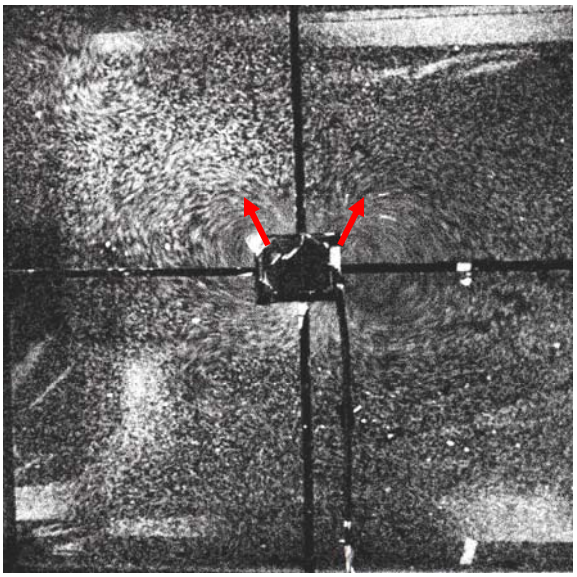

Figure 2.4 (a) end of upstroke of 1st cycle

Figure 2.4 (b) end of downstroke of 1st cycle

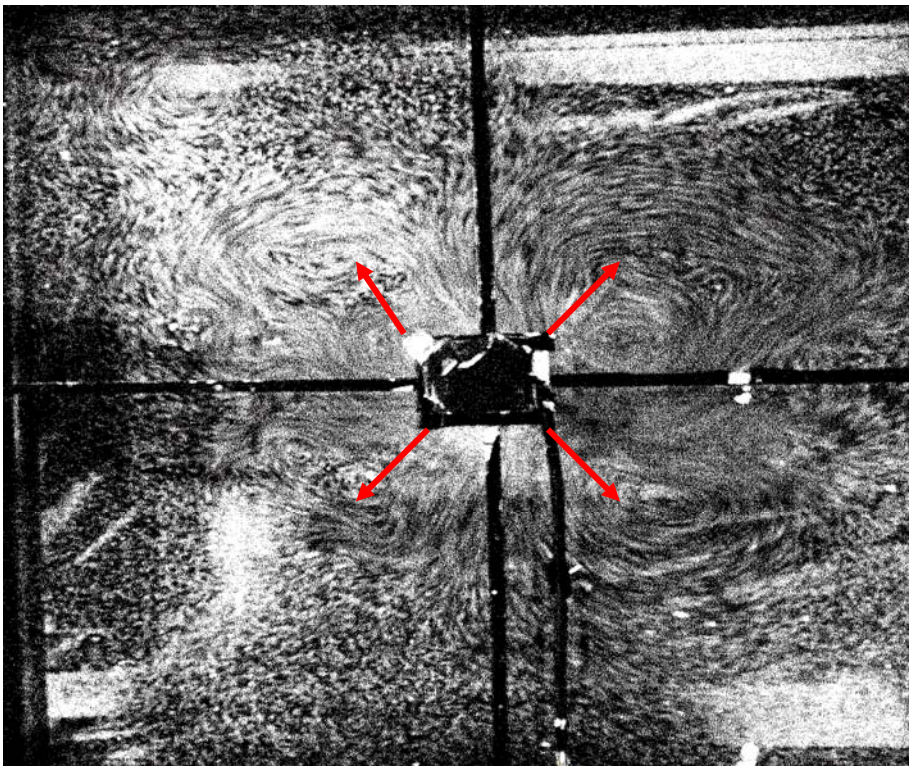

Figure 2.4 (c) end of 15th cycle

2.3.2 Asymmetric flapping with Φ=0:

By asymmetric flapping we mean that the downstroke speed is greater than the upstroke period. As the downward speed is greater the shedded wakes are advected downward due to the greater speed. As the wake vortices are having downward momentum at the end of each cycle the total upward momentum imparted to the wings is substantial and lift is generated. Figure 2.5 shows the wing configuration and velocity profile. Figure 2.6 shows flow structures at different cycles of the asymmetric flapping.

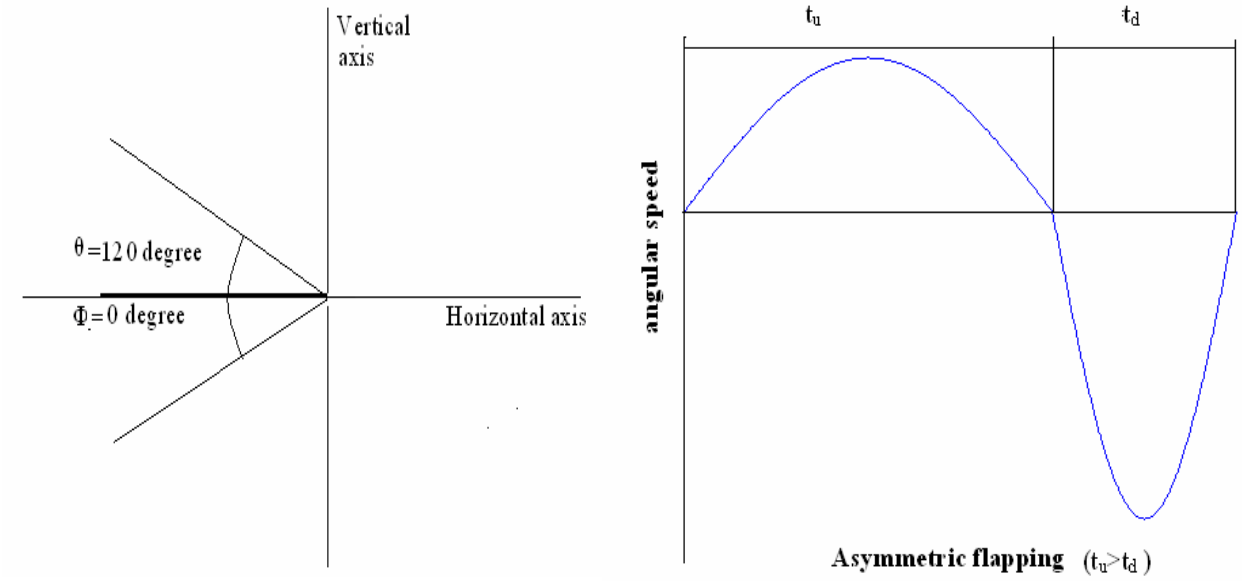

(a) **(b) t_u=14 sec; t_d=7 sec**

Fig 2.5 (a) wing configuration (b) velocity profile of the asymmetric flapping

In the fig 2.6 b and c two downward jets can be observed. By the time of 15th cycle although the downward jets are not distinct, the downward portion of the flow structure (fig 2.6 d) are having the greater share of vortices implying downward momentum transfer.

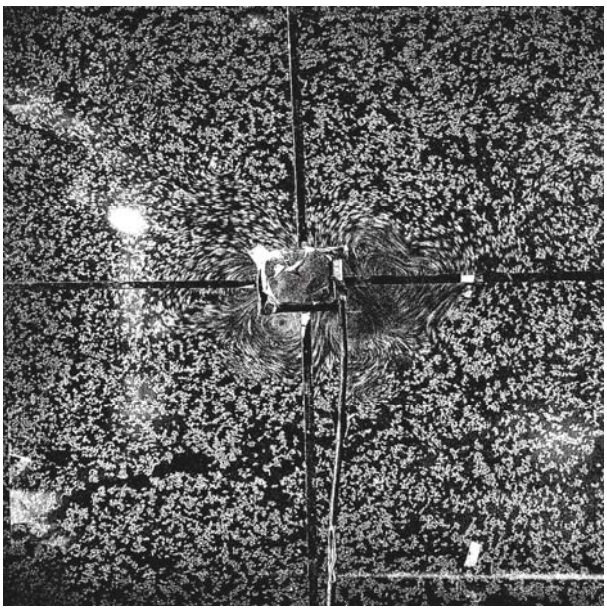

Fig2.6 (a) first cycle

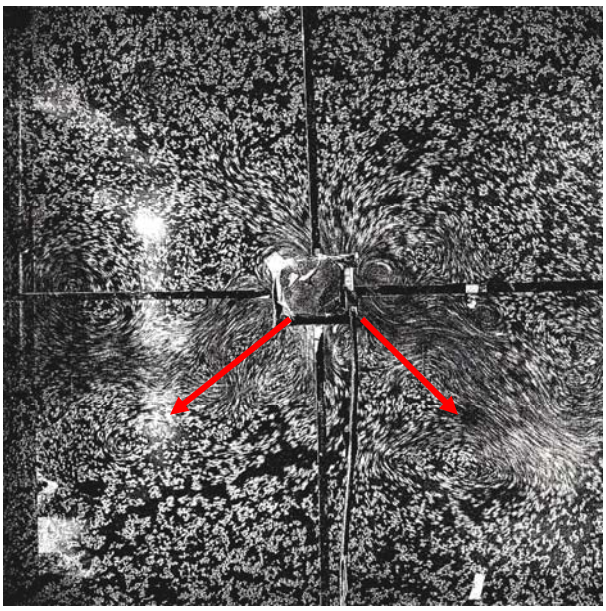

Fig2.6 (b) fifth cycle

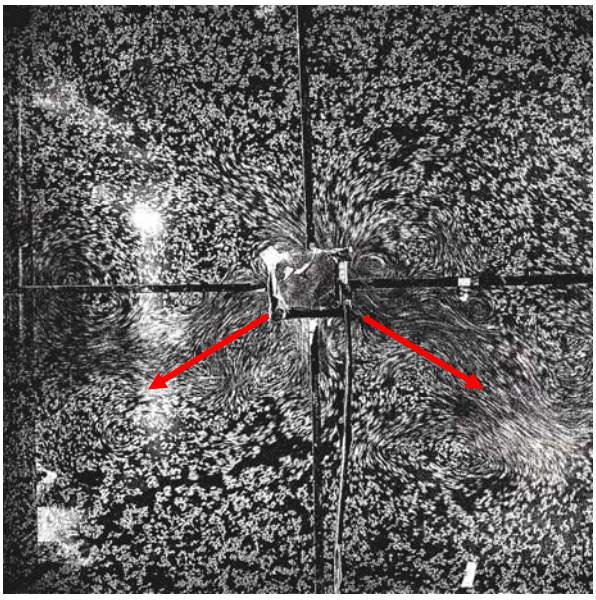

Fig2.6 (c) tenth cycle

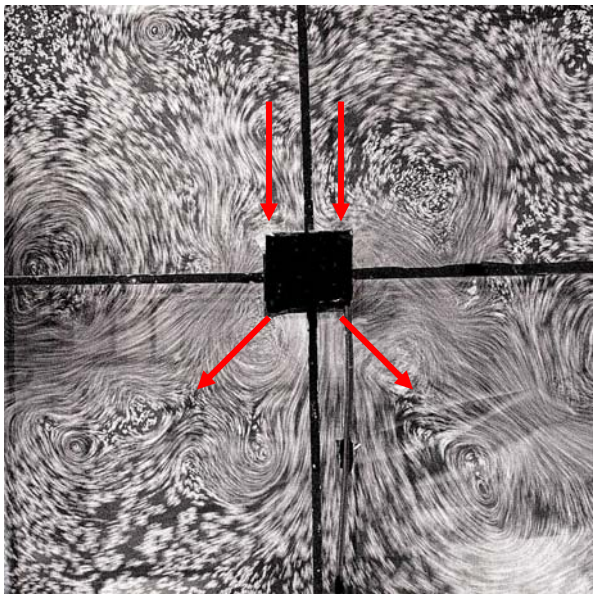

Fig2.6 (d) fifteenth cycle

2.3.3 Symmetric flapping with mean position inclined to horizontal axis

The two results presented in previous sections are earlier shown by Shreyas (2005). Our aim is to find out the influence of the mean position of the wing on lift. Even in the case of symmetric flapping, with the mean position of the wing inclined to horizontal axis at certain degree, lift is generated. Figure 2.7 represents the wing configuration and the velocity profile.

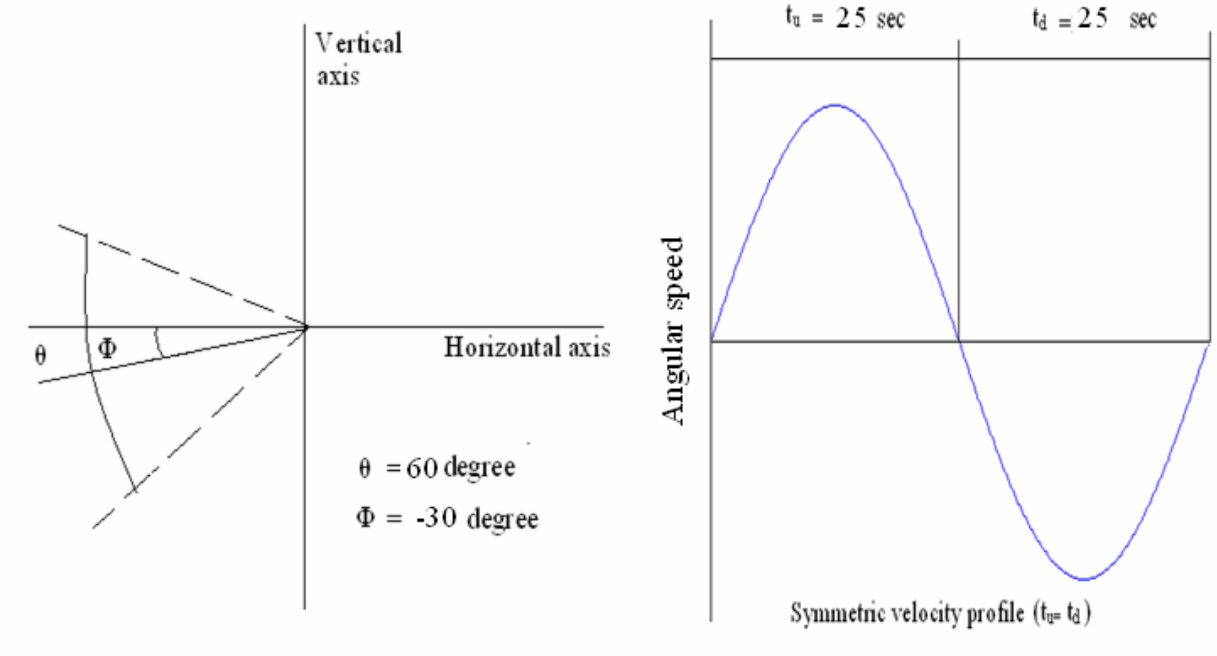

(a) **(b)**

Fig 2.7 (a) wing configuration (b) velocity profile of the symmetric flapping

Figure 2.8 shows flow visualizations for symmetric flapping with mean position inclined to horizontal axis. Jets are pumped in downward direction which in turn imparts upward lift to the wings. In the next chapter, through numerical simulation it has been shown that even in symmetric flapping lift is generated with the mean position inclined to horizontal axis.

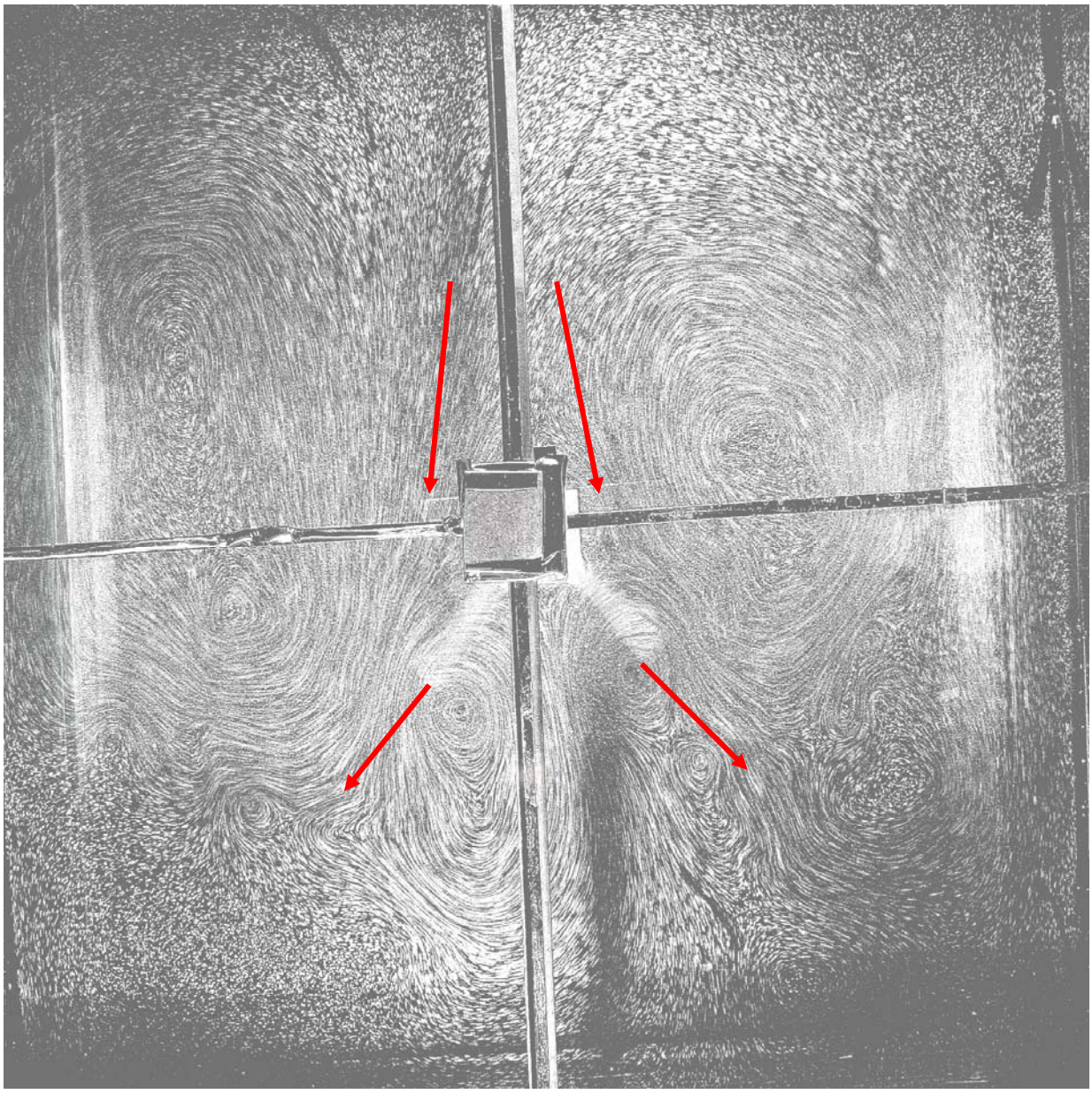

Fig 2.8 Symmetric flapping with Φ= -60^{o} and θ=60^{o} at 10th cycle; chord length c=14 cm

2.3.4 Asymmetric flapping with mean position inclined to horizontal axis:

If inclined mean position increases the lift generation for the symmetric flapping it will surely enhance lift for asymmetric flapping as substantial lift is already generated with the mean position aligned with the horizontal axis. Figure 2.9 shows the wing configuration and the velocity profile.

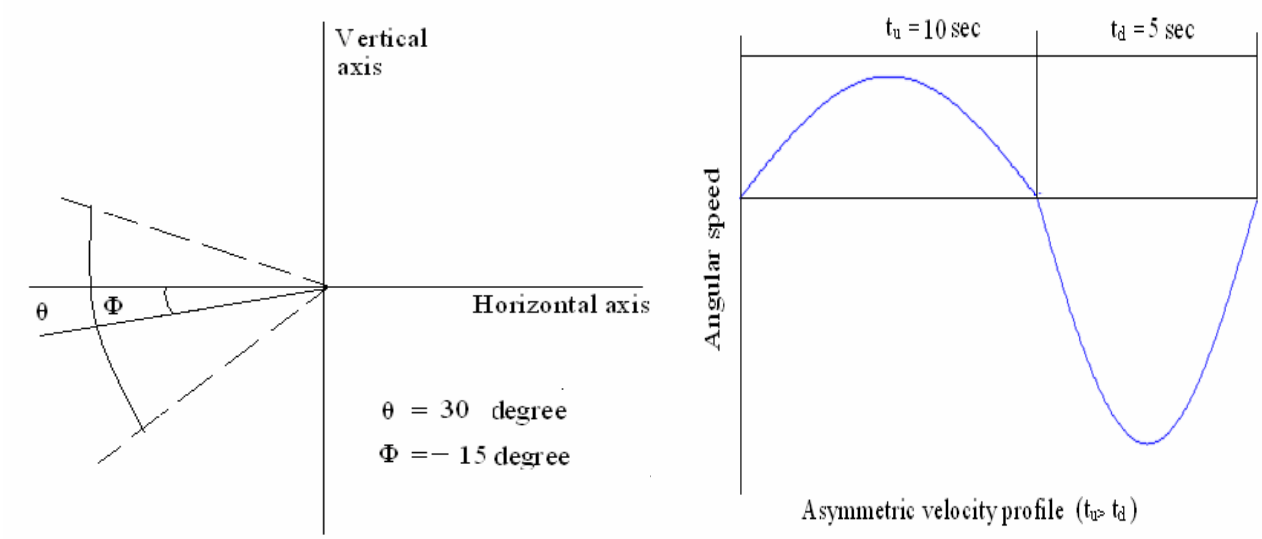

Fig 2.9 (a) wing configuration (b) velocity profile

Fig 2.10 represents the flow structure at the end of the 10^{th} cycle with Φ=-15^o. It can be observed that the two outgoing jets are inclined around -15^o with respect to horizontal axis. Figure 2.11 shows the flow diagram when the mean position is at Φ=-60^o and the angular amplitude is 60^o. The jets in Fig 2.11 are clearly having greater downward component than that of fig 2. 10. Although we can't make any quantitative statement from these figures numerical simulations in the next chapter shows that the inclination of the mean position substantially increases lift. Also it is shown through simulation that with the increase of mean position w.r.t horizontal axis lift is enhanced. Results of flow visualization presented in Figures 2.8 & 2.11 are done with Aditya K as part of his summer internship. In the figure 2.11 wings flap between -30^o -90^o. As a result the wake vortices of each wing interact with each other strongly.

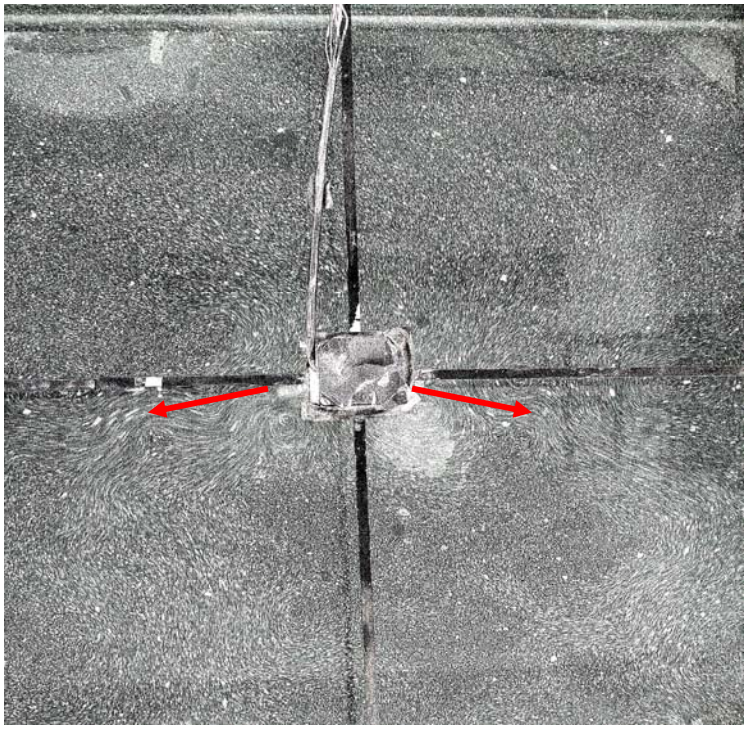

Fig 2.10 at end of 10th cycle Φ=-15^{o}; θ=30^{o}; c=8cm

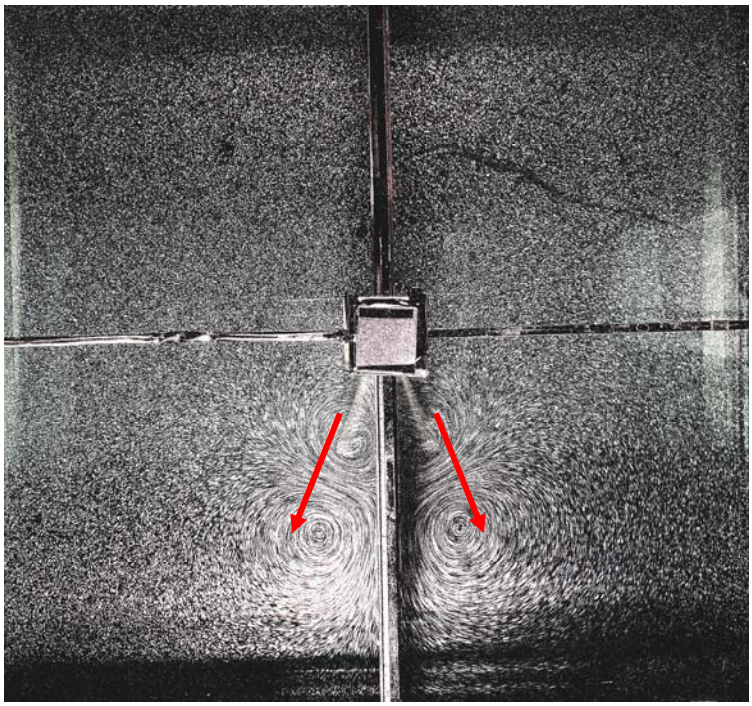

Fig 2.11 at end of 5th cycle Φ=-60^{o}; θ=60^{o}; c=14 cm

CHAPTER 3

NUMERICAL SIMULATION

In the last chapter experimental results were presented to gain qualitative insight into lift production in flapping flight. To get quantitative information two dimensional numerical simulation of flapping wings using discrete vortex method are carried out. We have used inviscid and well as incompressible flow conditions. The discrete vortex method has some advantages:

1. In this scheme we need to solve only those regions of the flow where vortices are Located, whereas other methods require to solve the whole flow field.
2. As the wings are flapping, grid generation is required in the grid based methods in each time step. In vortex method we don't require grid generation which saves computational complexities and simulation time.

One problem with vortex method is, as it is a N body problem which needs mutual interaction of N particles. Thus computation cost increase enormously with number of vortex bodies. However this drawback can be solved by implementing the Fast multipole method (FMP).

3.1 Basic formulation of Discrete Vortex Method

The governing Navier Stokes equation is

$$\frac{\partial u}{\partial t} + u.\nabla u = -\frac{1}{\rho}\nabla p + \nu\nabla^2 u \qquad (3.1.1)$$

In this equation there is pressure term, to eliminate p let u ($\vec{x}$,t) be the velocity field and $\Omega(\vec{x},t) = \nabla u(\vec{x},t)$ be the vorticity field. By taking curl of the equation (3.1.1) the vorticity transport equation is obtained; which is :

$$\frac{\partial \Omega}{\partial t} + u.\nabla\Omega = \Omega.\nabla u + \nu\nabla^2\Omega \qquad (3.1.2)$$

The first term on the right hand side of 3.1.2 is vortex stretching and vortex tilting. As our simulations are confined to 2D, this term will be zero. Under inviscid assumptions the second term in the right hand side can be neglected. In our simulation, we have used constant density flow, conservative body forces and unbounded region. So the equation (3.1.2) reduces to:

$$\frac{D\Omega}{Dt} = 0 \qquad (3.1.3)$$

where $\frac{D}{Dt}$ is material derivative. This leads to basic formulation of vortex method for which Lagrangian method based on elements of vorticity has been adopted. In the simulations, point vortices have been avoided as point vortices have singularities and mutual interaction of two point vortices at very small distance may blow up the solution, instead vortex blobs are used .The total vorticity field is expressed as the summation of individual vortex blobs as follows:

$$\vec{\Omega}(\vec{x},t) = \sum_{i=1}^{N} \Gamma_i(t)\zeta_{\sigma_i}(\vec{x} - \vec{x}_i(t)) \qquad (3.1.4)$$

where Γ_i is the circulation strength of vortex particle. ζ_{σ_i} represents the distribution of the vorticity and is called cutoff function. For vortex blobs cut off function assumes Gaussian distribution having uniform core size ($\sigma_i = \sigma$). The cut off function in 2 D is expressed as:

$$\zeta_{\sigma_i} = \frac{1}{k\pi\sigma^2}\exp\left(-\frac{|\vec{x}|^2}{k\sigma^2}\right) \qquad (3.1.5)$$

where k represents the width of the cutoff. For 'k' although different authors have suggested 1, 2 or 4, we have used k=1 in our simulations. As per inviscid condition the vortices convect with the local velocity without any deformation.

Now using Biot-Savart law velocity can be obtained as:

$$q = \frac{\Gamma}{4\pi}\int \frac{d\vec{l} \times (\vec{r}_0 - \vec{r}_1)}{|\vec{r}_0 - \vec{r}_1|^3} \qquad (3.1.6)$$

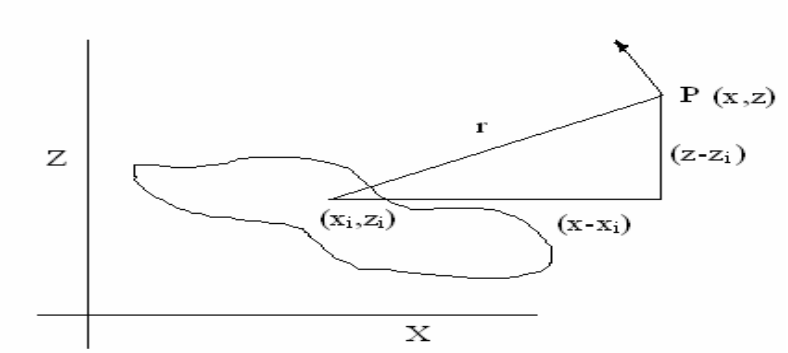

Fig 3.1 Velocity at point P due to vortex distribution

For 2-D vortex blob the velocity (u,w) is as follows:

$$\begin{pmatrix} u \\ w \end{pmatrix} = \frac{\Gamma}{2\pi r^2}\begin{pmatrix} z - z_i \\ x_i - x \end{pmatrix}(1 - \exp(-\frac{r^2}{\sigma^2})) \qquad (3.1.7)$$

Where $r^2 = (x - x_i)^2 + (z - z_i)^2$ and σ is the vortex core radius.

Now the Lagrangian form of vortex method in 2D can be expressed as

$$\frac{dx_i}{dt} = u(x_i, t) \qquad (3.1.8)$$

We have used no normal flow condition as boundary condition. Using the equation (3.1.8), we calculate velocity of the individual particles taking into account the mutual interaction of the shedded wake vortices and vortices on the wing using Biot-Savart law. It has been shown in t-he simulations of 2D flow (Wang 2000, Hamdani & Sun 2000) and 3D flows(Rammurti & S-andberg 2002) airfoils show a remarkable similarity in forces calculated at Reynolds number 100 and 100000.These results motivated us to adopt 2D simulations without viscosity effect w-hich is also bolstered by the empirical data (Usherwood & Ellington 2002,b). Even though our simulations are "inviscid", very fact that we take a finite vortex core for vortex blob implies v-iscous effect. The core size σ is related to viscosity and time steps as follows:

$\sigma = 2\pi\sqrt{\nu\Delta t} \Rightarrow \nu = \sqrt{\frac{\sigma^2}{4\pi^2} \times \frac{1}{\Delta t}}$ represents fluid viscosity in our simulations.

3.2 *Numerical implementation of discrete vortex method*

In this section we have discussed the implementation of vortex method for flapping wings.

3.2.1 Definition *of geometry*

The two wings considered in our simulations are being modeled as the flat plates used in our experiments. As the simulation is 2D, we don't consider third dimension i.e. any length along the axis of rotation.

3.2.2 Choice of singularity

In our simulation we have used vortex blobs instead of point vortices. Point vortices are avoided because mutual interaction of two vortices at very close distance will cause huge fluctuations a singularity. So we have used the vortex blobs described in the equations (3.1.7). We represent the wing surface as a series of discrete vortices on each panel's quarter point. The shedded wakes are also modeled as vortex blobs.

3.2.3 Kinematics

The angular velocity of the flapping wing is given as

$$\theta = \frac{\theta}{2}\sin(\omega t) \quad \dot{\theta} = \frac{\theta}{2}\omega\cos(\omega t) \tag{3.2.1}$$

where θ is angular amplitude and ω is angular frequency. Each time step (Δt) is taken to be 0.001 sec. The distance of the shedding from the chord tip is $0.3U_{\infty}\Delta t$ along the chord length.

3.2.4 Discretization of geometry

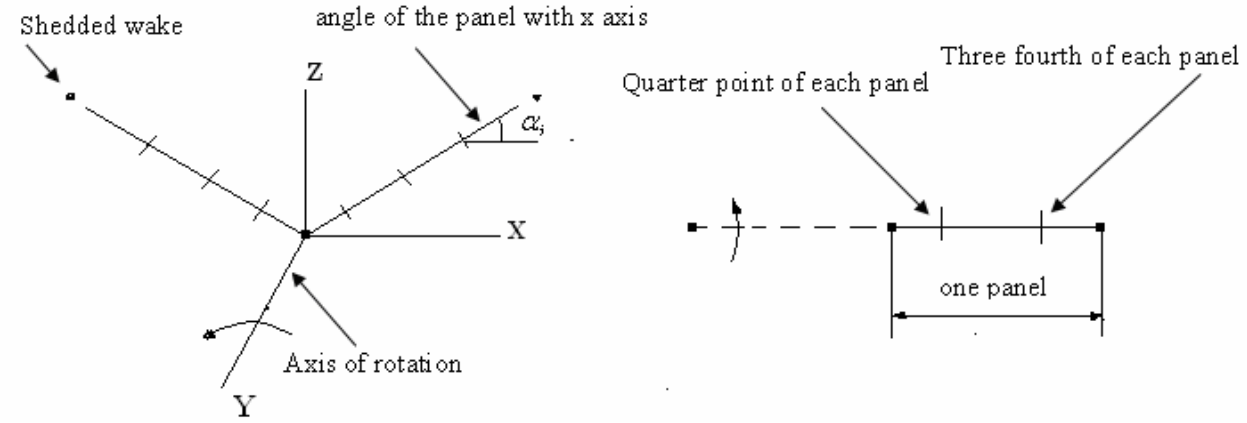

Fig 3.2 Discretization of the wings into panels and description of each panel

Each wing is divided into N panels of equal length. For our simulation we have generally used 10 panels for unit chord length 1. At each panel's quarter point vortices are placed

and at each three quarter point of a panel termed as collocation point, we are implementing no normal flow boundary condition. For each collocation point the local normal vector has to be calculated. The normal n_i at each collocation point is calculated as **:**

$$n_i = \frac{(-\frac{d\eta_i}{dx},1)}{\sqrt{\left(\left(\frac{d\eta}{dx}\right)^2+1\right)}} = (\sin\alpha_i, \cos\alpha_i) \tag{3.2.2}$$

If the wing is rigid and planar α_i is same for all panels for an individual time step. However for flexible wings α_i is to be calculated for each individual panel.

3.2.5 Influence coefficients

Influence coefficient is defined as the normal velocity induced at the collocation point by a panel of unit circulation strength. So for a unit strength vortex element j the influence coefficient at i^{th} collocation point is

$$a_{ij} = (u, w)_{ij} . n_i \tag{3.2.3}$$

Thus the set of algebraic equations are as follows:

$$\begin{bmatrix} a_{11} & a_{12} & . & . & . & . & a_{1N} & a_{1W} \\ a_{21} & a_{22} & . & . & . & . & a_{2N} & a_{2W} \\ . & & & & & & & . \\ . & & & & & & & . \\ . & & & & & & & . \\ . & & & & & & & . \\ a_{N1} & a_{N2} & . & . & . & . & a_{NN} & a_{NW} \\ 1 & 1 & 1 & . & . & . & 1 & 1 \end{bmatrix} \begin{Bmatrix} \Gamma_1 \\ \Gamma_2 \\ . \\ . \\ . \\ . \\ \Gamma_N \\ \Gamma_{wi} \end{Bmatrix} = \begin{Bmatrix} RHS_1 \\ RHS_2 \\ . \\ . \\ . \\ . \\ RHS_N \\ \Gamma(t-\Delta t) \end{Bmatrix} \tag{3.2.4}$$

The influence coefficients a_{11} to a_{1N} are due to contribution of 1 to N^{th} panel vortices on 1^{st} collocation point. The influence coefficient a_{iw} is contributions from the latest wake vortices at each time step. Now according to Kelvin's circulation theorem it is known that in a inviscid barotropic flow with conservative body forces the net circulation around a closed curve moving with the fluid remains constant with the time i.e. $\frac{D\Gamma}{Dt} = 0$.

So from the set of equations in (3.2.4) the last equation represents the Kelvin condition

$\Gamma(t)-\Gamma(t-\Delta t)+\Gamma_{w_i}=0$ where $\Gamma(t)=\sum_{i=1}^{N}\Gamma_i$ is the net circulation of N panels at the time 't'.

(3.2.5)

The right hand side equation represents the normal flow velocity induced by previous shedded wakes and the wing motion**:**

$$RHS_i=-\left[U(t)+u_w,W(t)+w_w\right]_i.n_i \qquad (3.2.6)$$

This set of equations represents the boundary conditions of our problem:

$$\left(\nabla\Phi_B+\nabla\Phi_W-\omega\times r\right).n=0 \qquad (3.2.7)$$

where the disturbance potential Φ is divided into wing potential Φ_B and wake potential Φ_w respectively and ω be the angular velocity and $\vec{r}$ is the position vector of the point on the wing.

So at each time step we have to calculate the influence coefficients. The set of (N+1) equations solves the circulation around the wings and the strength of the latest shedded vortex.

3.2.6 Force Calculations

It can be shown that pressure difference between upper and lower surface is (Katz):

$$\Delta p_j=\rho\left(U_\infty\frac{\Gamma_j}{\Delta l_j}+\frac{\partial}{\partial t}\sum_{k=1}^{j}\Gamma_k\right) \qquad (3.2.8)$$

where Γ_j is the circulation around each panel, Δl_j is the length of each panel, U_∞ is the free stream velocity. We have used half of wing tip velocity as U_∞. The 2nd term is time derivative of the sum of vortices from leading edge to j^{th} panel. Since the 2nd term on being multiplied with air density at 20°C (1.2×10^{-3} gm/cm^3) becomes much smaller in comparison to the 1st term it is neglected during lift calculation. Also when time averaged lift calculation is done considering both the terms there seems to be difference in second order with the lift calculated using the first term only.

The total lift is obtained by integrating the pressure difference along the chord length**:**

$$L=F_z=\sum_{j=1}^{N}\Delta p_j\Delta l_j\cos(\alpha_j) \qquad (3.2.9)$$

A flow chart is given in Fig (3.2).

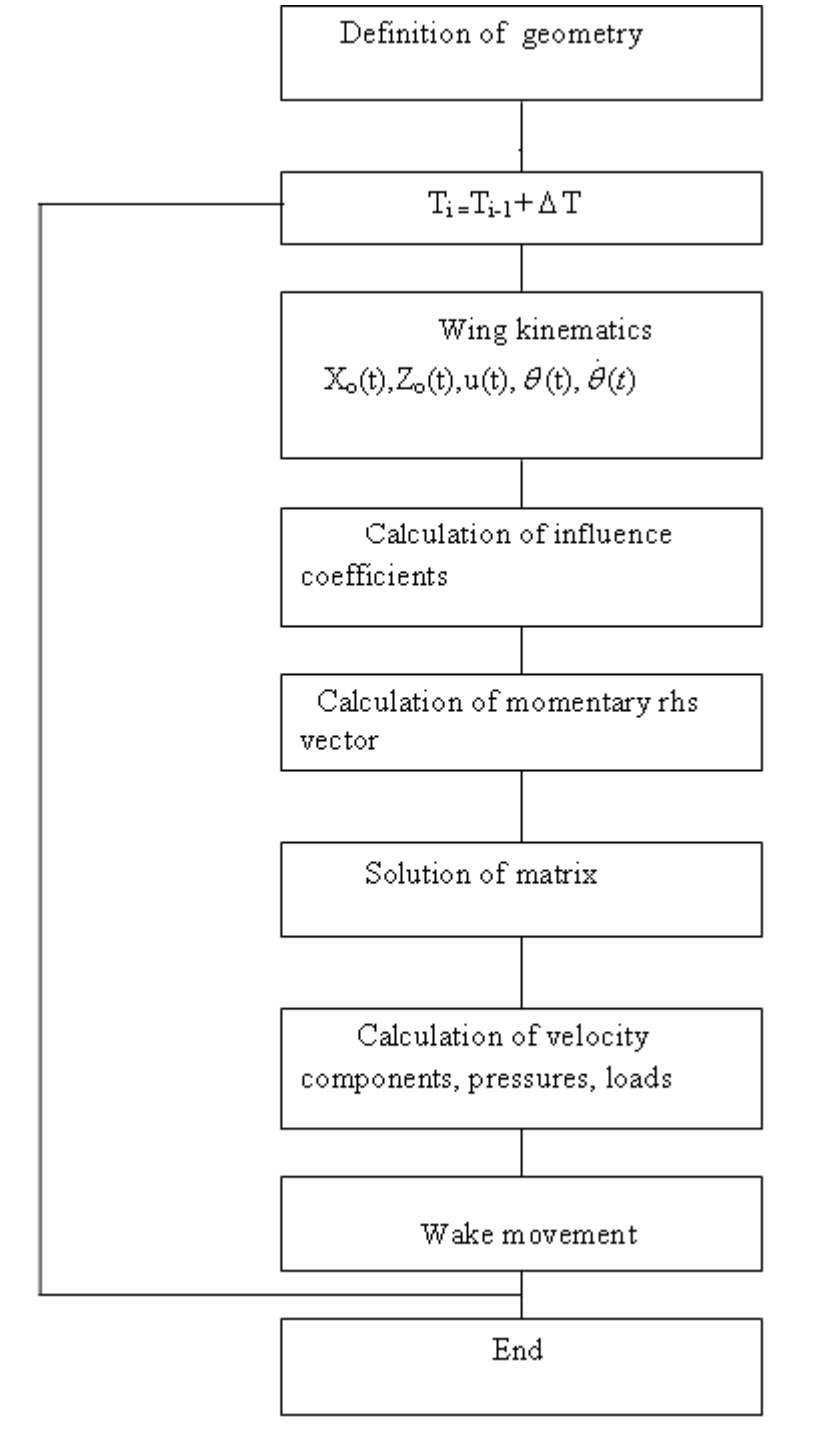

Fig. 3.3 Algorithm of discrete vortex method for flapping wing

3.2.7 Wake Movements

After the solution of the equations (3.2.4) the movement of the wakes are calculated. According to Biot Savart law each vortex must move with the local velocity which is the summation of the velocity components induced by the wing and other shedded vortices. During each time step their new locations are calculated as follows:

$$(\Delta x, \Delta z)_i = (u, w)_i \Delta t \qquad (3.2.10)$$

We have run our programme using Matlab 7.1 on dual core processor, 2.67 GHz,3 GB RAM. For 1000 time steps implying 2×1000 shedded vortices computation time generally takes 20 minutes. As vortex method involves many-body interaction problem computation time increases with increase of number of time steps. It generally takes 2 hours for marching 2000 time steps. Due to RAM constraint we can't go beyond 2500 time steps. However, it is our speculation that FORTRAN programming will save computational time and more time steps can be done.

3.3 Results and discussions

In this section we will present simulation results indicating velocity field, vorticity field, time averaged lift diagrams and discuss the effects of different parameters like inclination (Φ), angular amplitude (θ), flexibility and ratio between upstroke speed to downstroke speed (AR) on lift magnitude.

3.3.1 Symmetric flapping

In symmetric flapping, we have observed the velocity fields at different cycles. When the wings are in the horizontal position after each cycle, in each quadrant of the velocity field we observe vortices of the opposite sign resulting in net circulation of zero. In fig 3.4 we have shown the velocity field at first cycle. In the first cycle the growth of circulation around wings can be observed. It has been highlighted that with upstroke there are shedded wakes behind

the wing. With the start of downstroke the shedded vortices are present both in upward half and downward half. In the final stages it is observed that in four quadrants, of the velocity field circulations of the opposite nature are present. In figure 3.5, we have shown the evolution of the velocity field at different cycles. Observing the velocity field, it can be inferred that the four directional jets are observed. This indicates that over a cycle zero-net upward momentum transfer and have zero lift. In figure 3.6 the variation of lift(dyne) in the case of symmetric flapping is present and it's almost symmetric about the x axis .

Now we have calculated time averaged non dimensional force $\bar{L} = \frac{1}{t}\int_0^t L.dt$

where $L = \frac{F_z t^2}{\rho c^3}$. (3.3.1)

F_z = vertical force dyne/cm length of the wing perpendicular to the plane

t = $(t_d + t_u)$ sec

ρ = 1.2×10^{-3} gm/cm^3

c = chord length, c =1 cm

In fig 3.7, we present the variation of $\bar{L}$ with time. From fig 3.7, it is evident that the time averaged force $\bar{L}$ is zero over 40 cycles is zero indicating zero lift. Hence the symmetric flapping produces four jets and zero-net force.

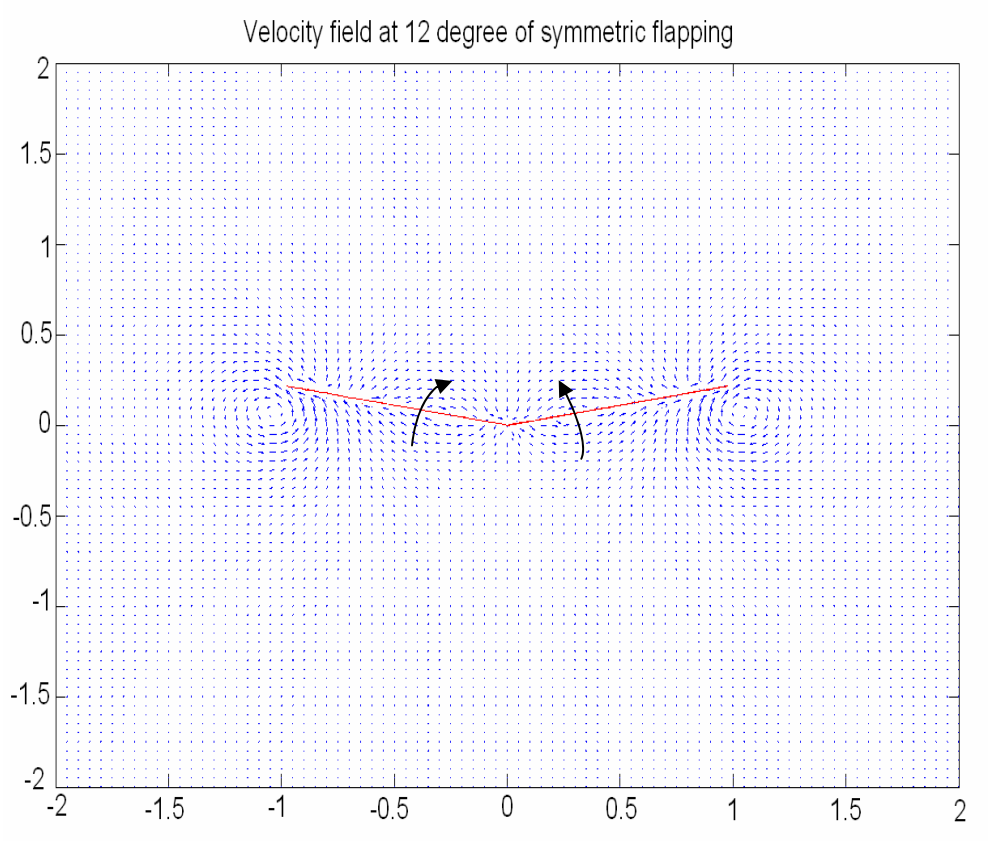

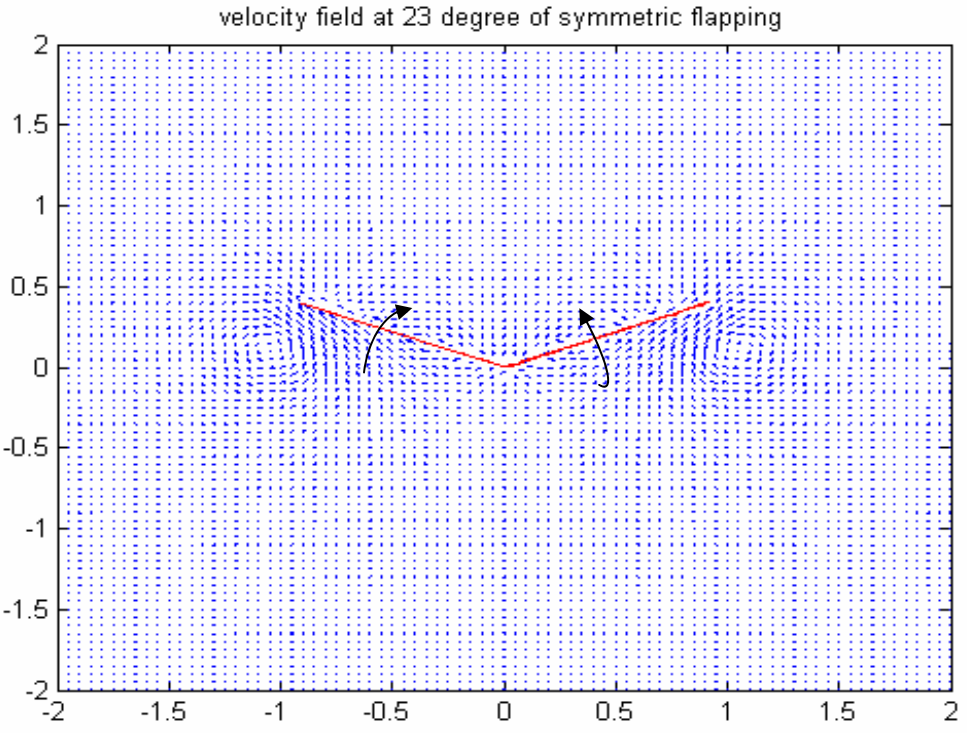

Fig 3.4 (a) velocity field during initial upstroke at 12º b) at 23º θ=80º; Φ=0º; t_d=0.017 sec; t_u=0.017 sec; AR=1;

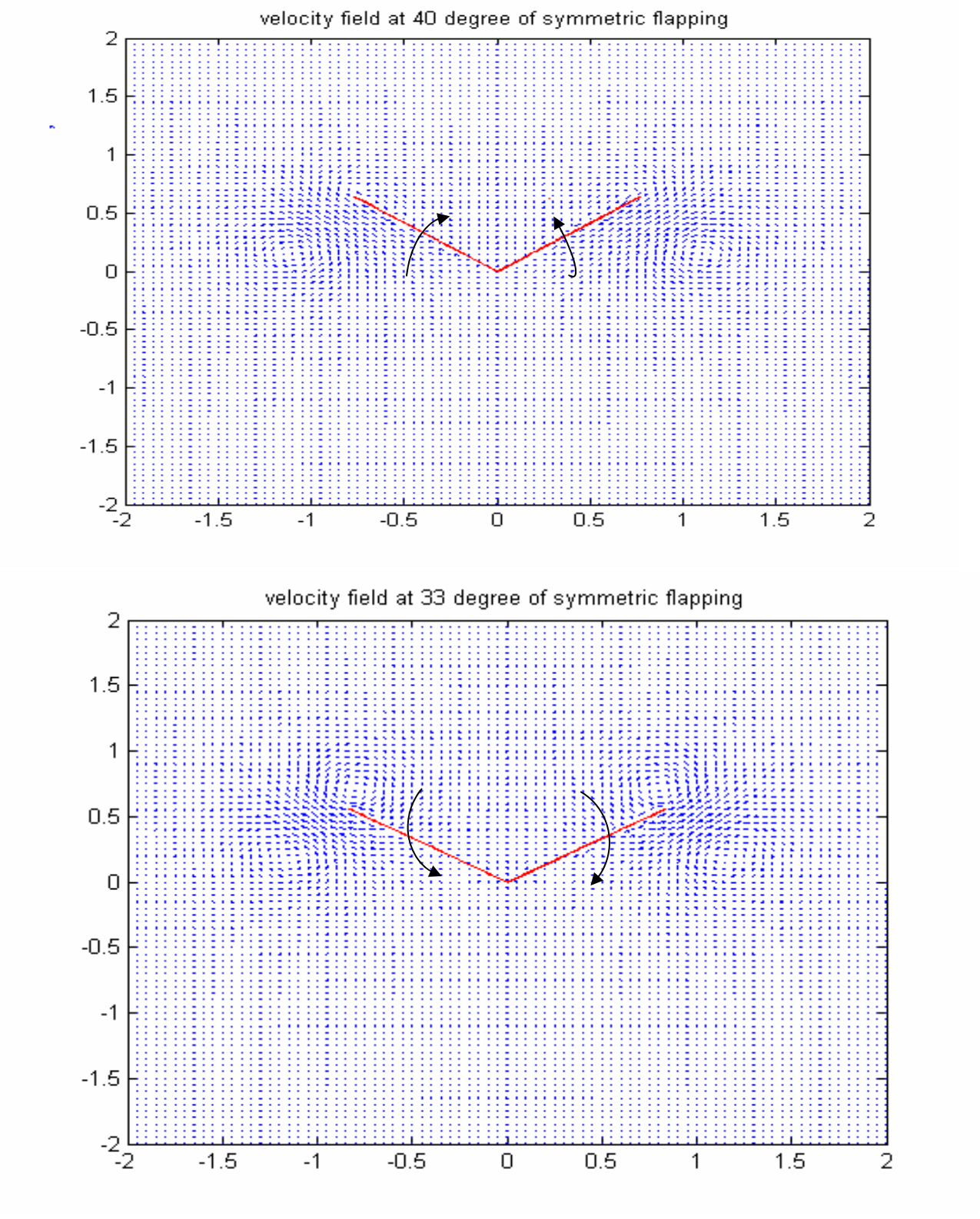

Fig 3.4 (c) velocity field during 40^o upstroke d) at 33^o downstroke θ=80^o; Φ=0^o; t_d=0.017 sec; t_u=0.017 sec; AR=1;

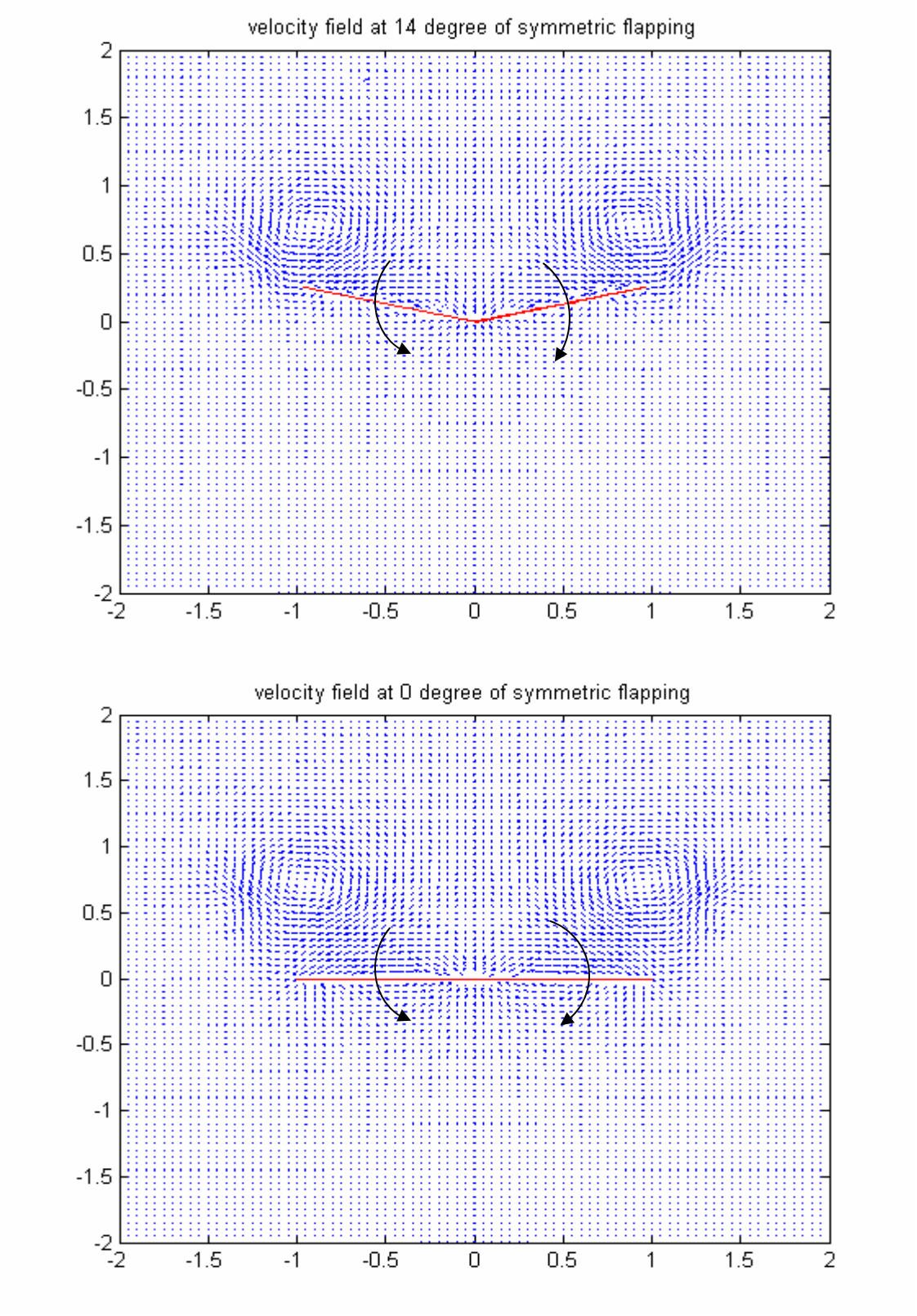

Fig 3.4 (e) velocity field during 14^o downstroke f) at 0^o downstroke θ=80^o; Φ=0^o; t_d=0.017 sec; t_u=0.017 sec; AR=1;

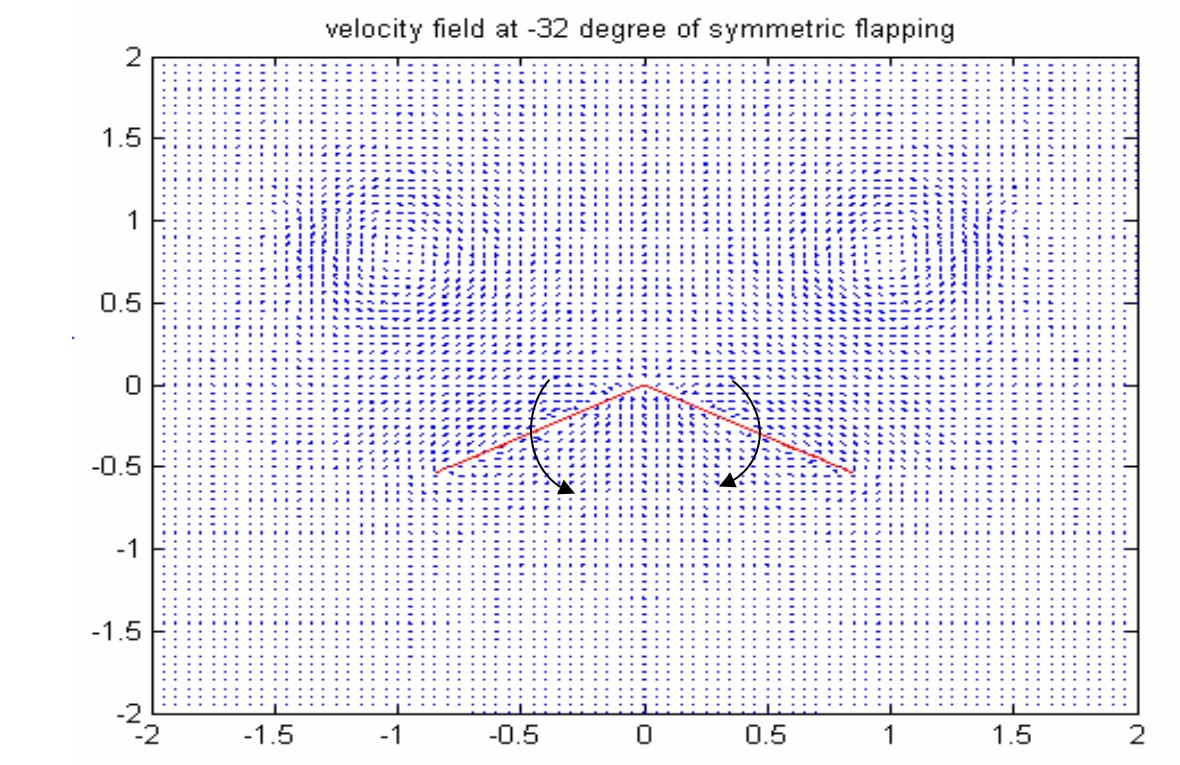

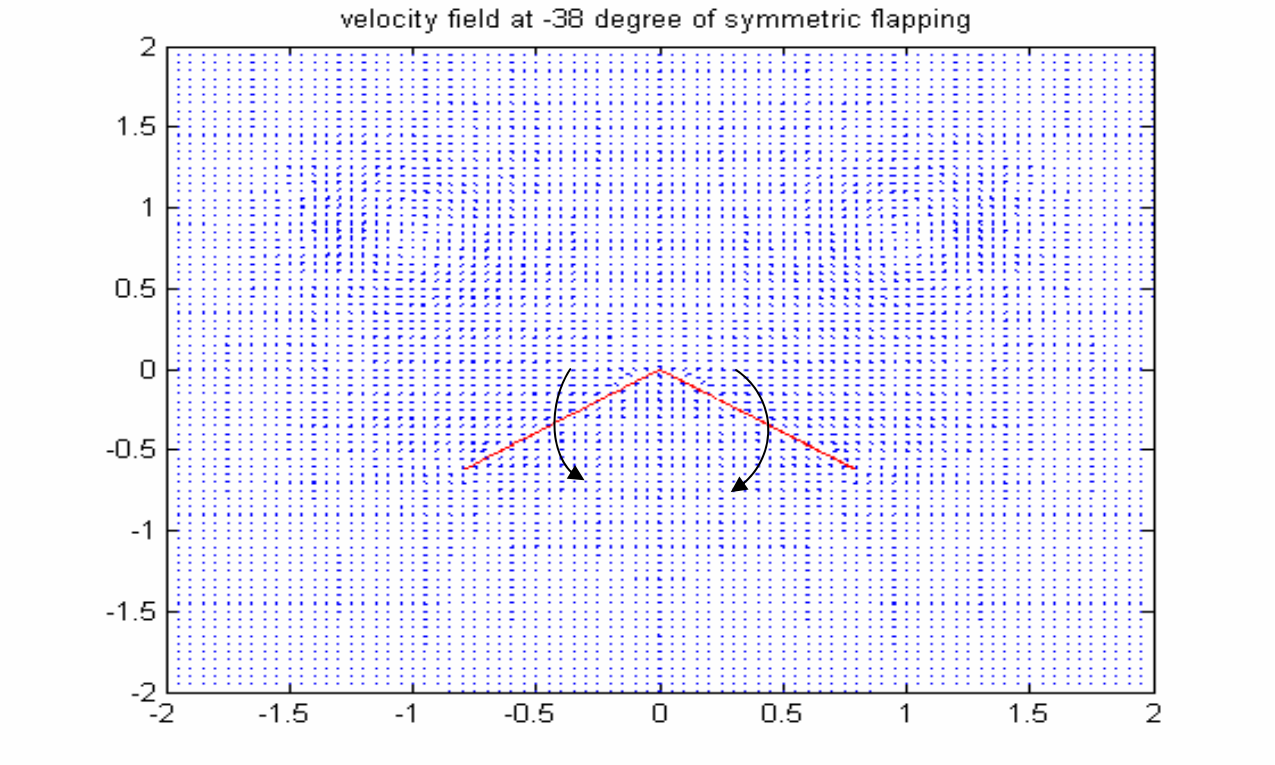

Fig 3.4 (g) velocity field during -32^o downstroke h) at -38^o downstroke θ=80^o; Φ=0^o; t_d=0.017 sec; t_u=0.017 sec; AR=1;

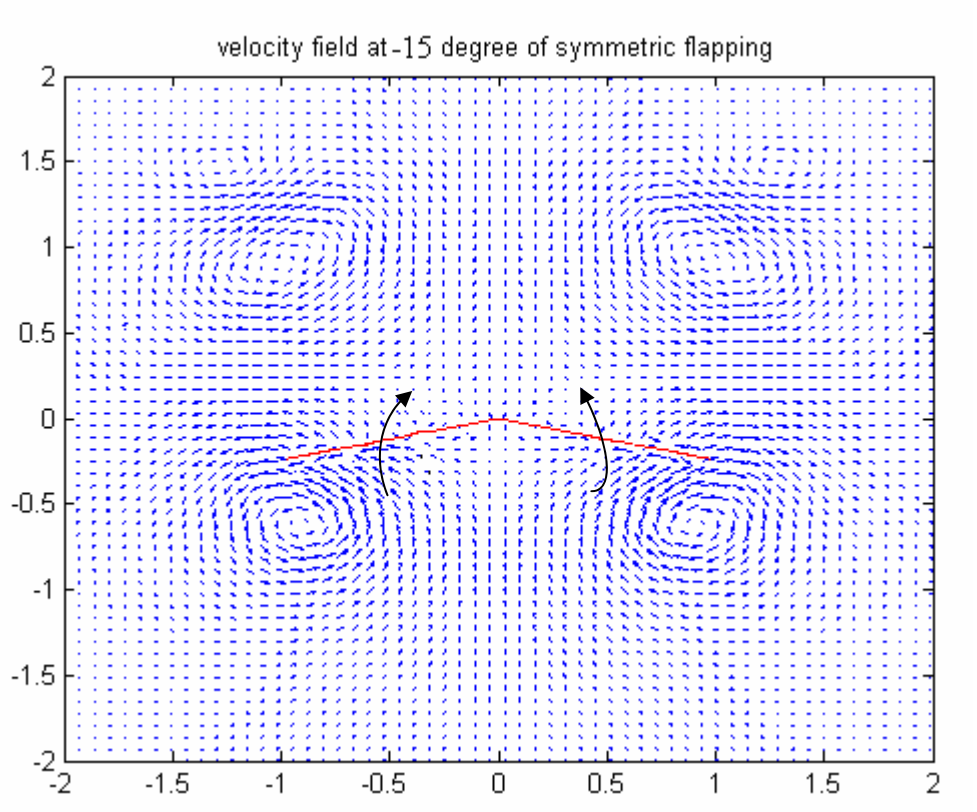

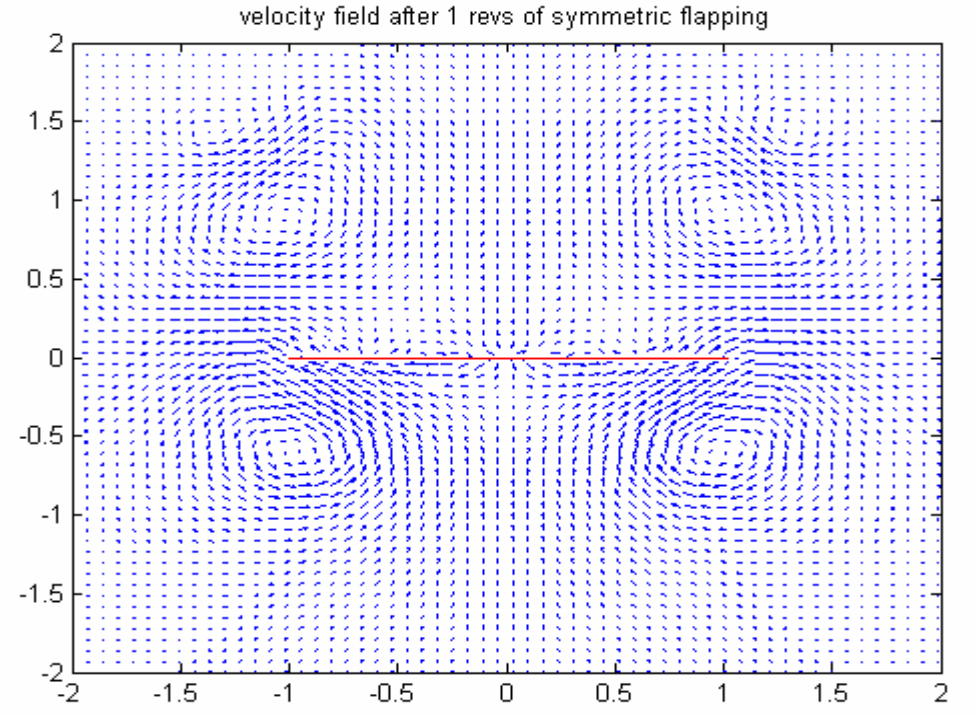

Fig 3.4 (i) velocity field during -35^o downstroke j) at -38^o downstroke θ=80^o; Φ=0^o; t_d=0.017 sec; t_u=0.017 sec; AR=1;

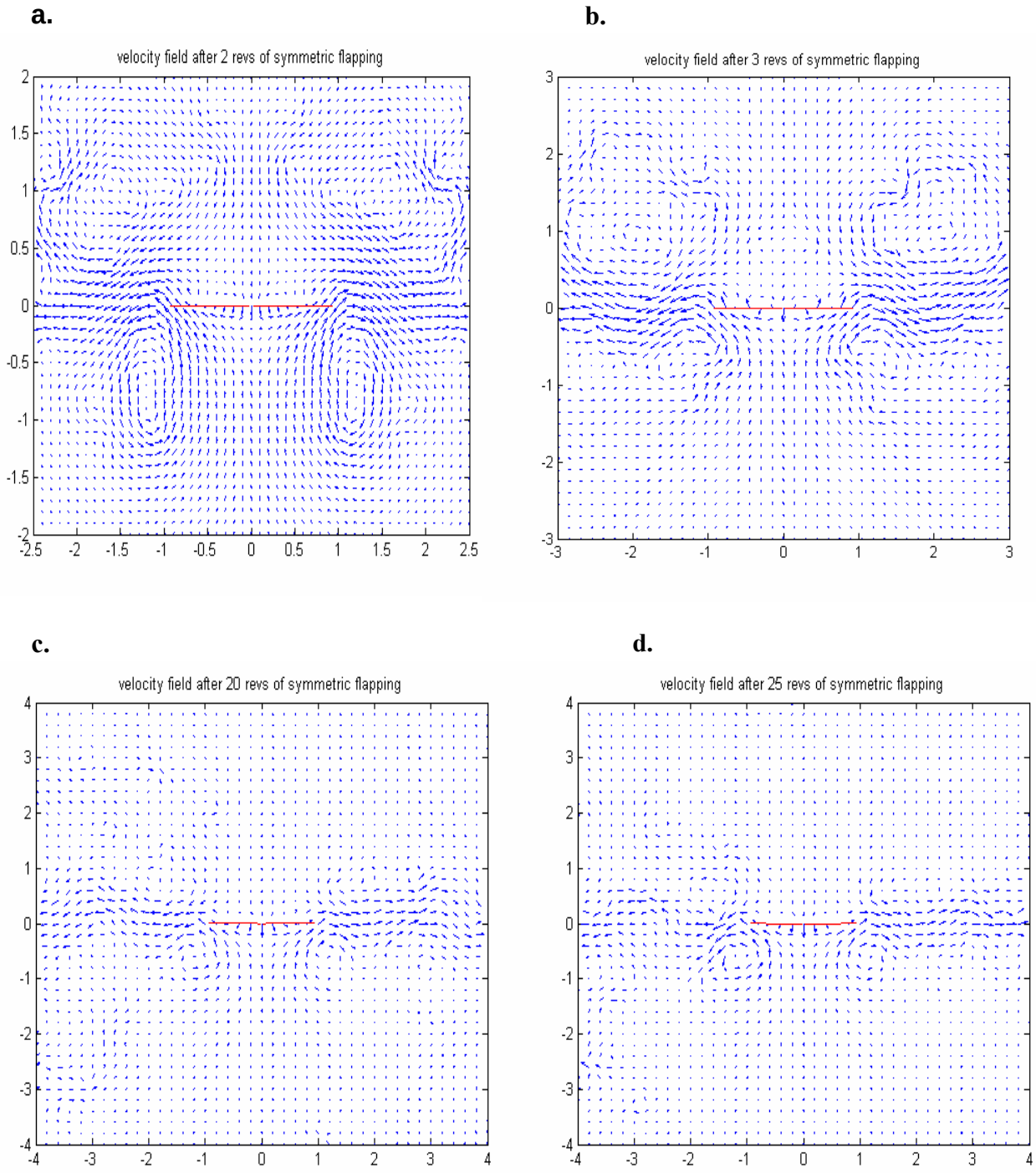

Fig 3.5 a) velocity field after 2 revolutions b) after 3 revolutions
c) after 20 revolutions d) after 25 revolutions
θ=80; Φ=0 degree; t_d=0.017 sec; t_u=0.017 sec; AR=1;

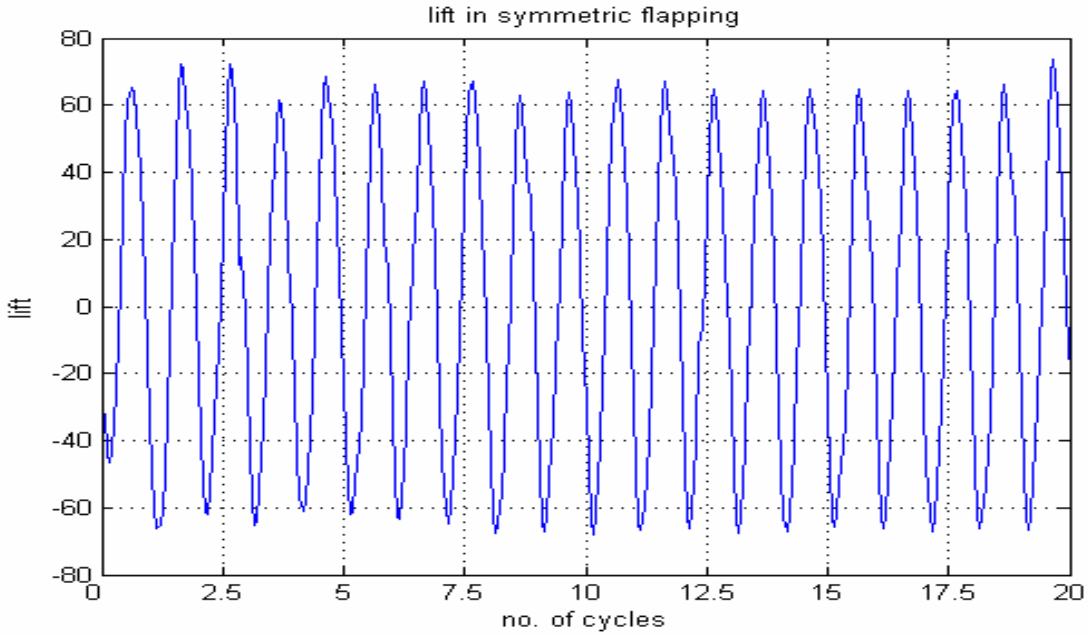

Fig 3.6 lift (dyne) over 20 cycles in case of symmetric flapping with θ=80^o angular amplitude, Φ=0^o and frequency of 20 rev/s

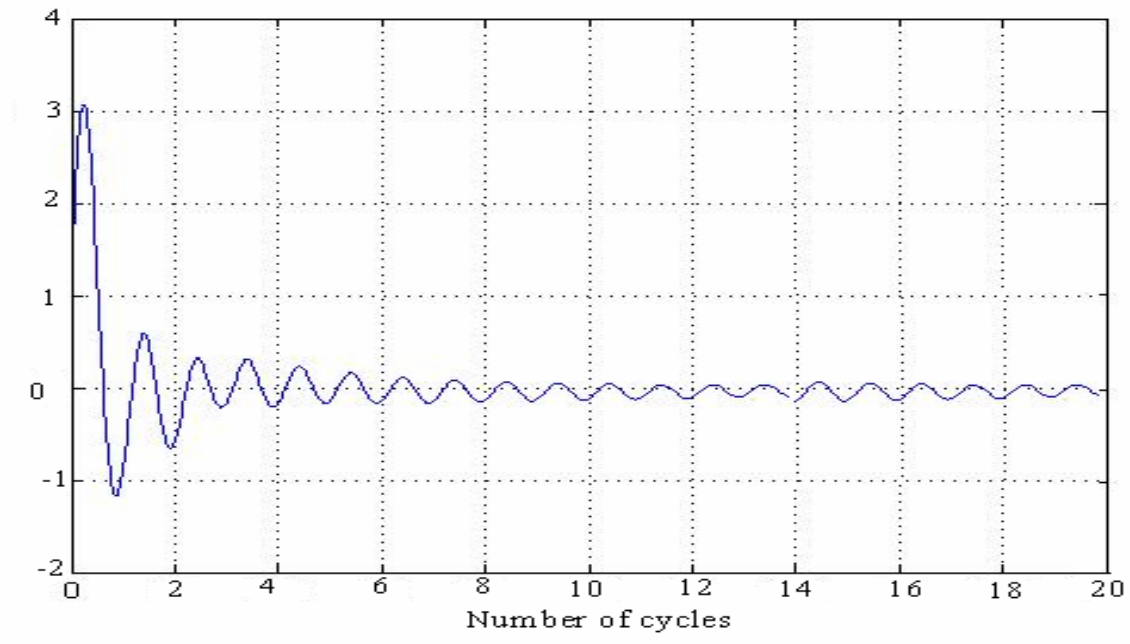

Fig 3.7 time averaged force $\bar{L}$ over 20 cycles of symmetric flapping with θ=80^o Angular amplitude, Φ=0^o and frequency of 20 rev/s

3.3.2 Effect of inclination in symmetric flapping

In the earlier section it is shown that if the mean position of the wings are at zero degree the time averaged force turns out to be zero. However one could explore the effect of Φ, i.e. inclination of the mean wing position inclination with respect to the horizontal axis on the lift. We present simulation results indicating flow field in which $\Phi=-20^o$; $\theta=80^o$ for symmetric flapping in figure 3.8. In figure 3.8a, we present velocity field for the similar symmetric flapping with $\Phi=0^o$. Here after 40 cycles we observe 2-jets moving horizontally. However when $\Phi=-20^o$, the direction of these jets are inclined to horizontal and is imparting downward momentum for the fluid. Thus we could say that even when the flapping is symmetric, if the inclination of mean-wing position is negative we could generate lift. Figure 3.9 presents the comparison of vorticity field and velocity contour for $\Phi=0^o$ and $\Phi=-20^o$. For $\Phi=-20^o$ it is observed that the shedded vortices are mostly in the downward half. In the velocity contour plots we observe that the zone of maximum velocity is inclined downward to the horizontal. Figure 3.10 shows the effect of inclination of the mean position w.r.t. horizontal axis on non dimensional lift. However, with symmetric flapping $\bar{L}$ is small but non zero.

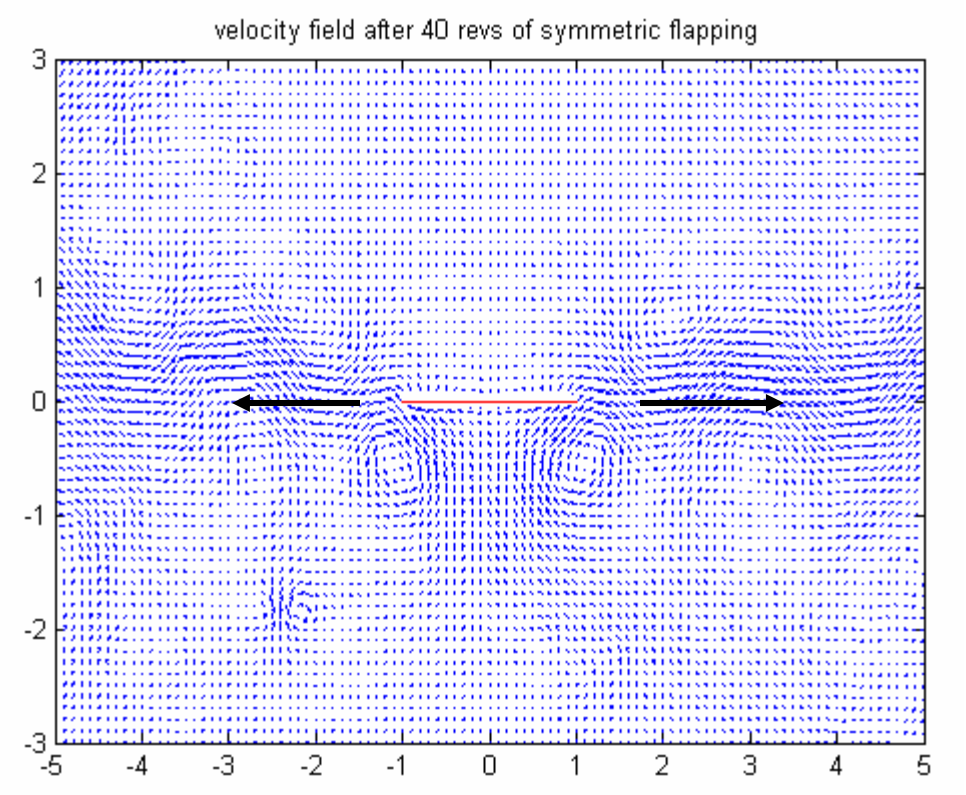

Fig 3.8 a. Velocity field after 40 revs of symmetric flapping with no inclination $\theta=80^o$; $\Phi=0^o$; $t_d=0.025$ sec; $t_u=0.025$ sec; AR=1;

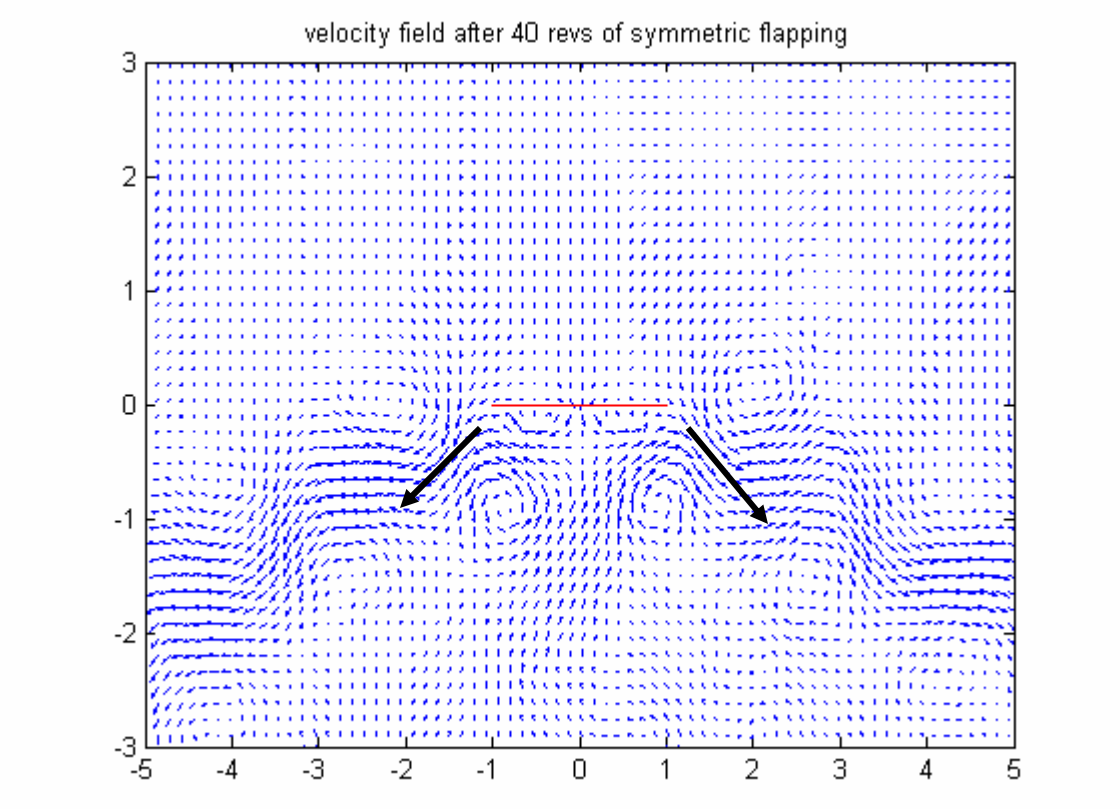

Fig 3.8 b. Velocity field after 40 revs of symmetric flapping with initial inclination of -20 degree $\theta=80^o$ degree; $\Phi=-20^o$; $t_d=0.025$ sec; $t_u=0.025$ sec; AR=1;

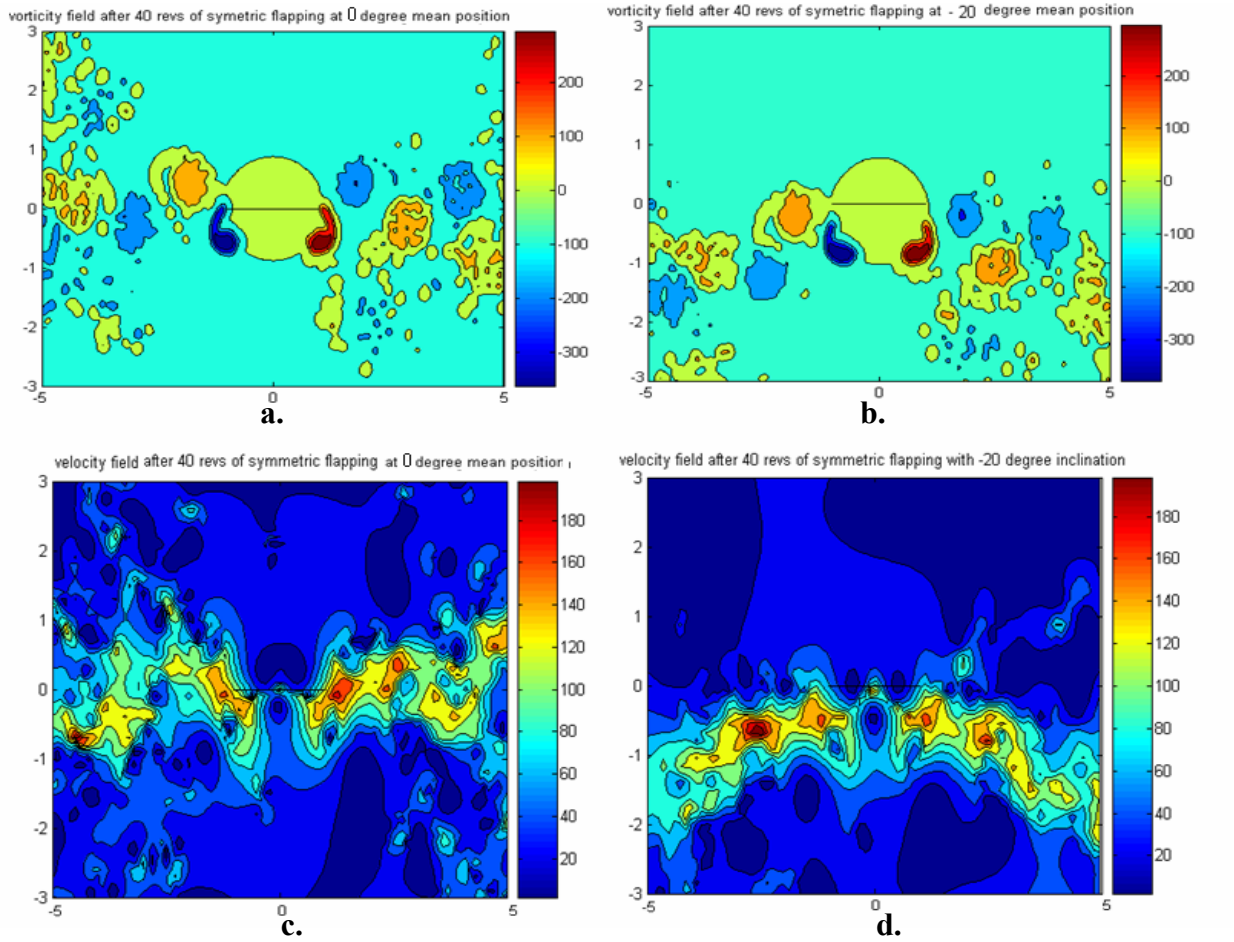

Fig 3.9 vorticity field at (a) Φ=0^o; (b)Φ=-20^o;
velocity contour plot at (c) Φ=0^o; (d)Φ=-20^o;

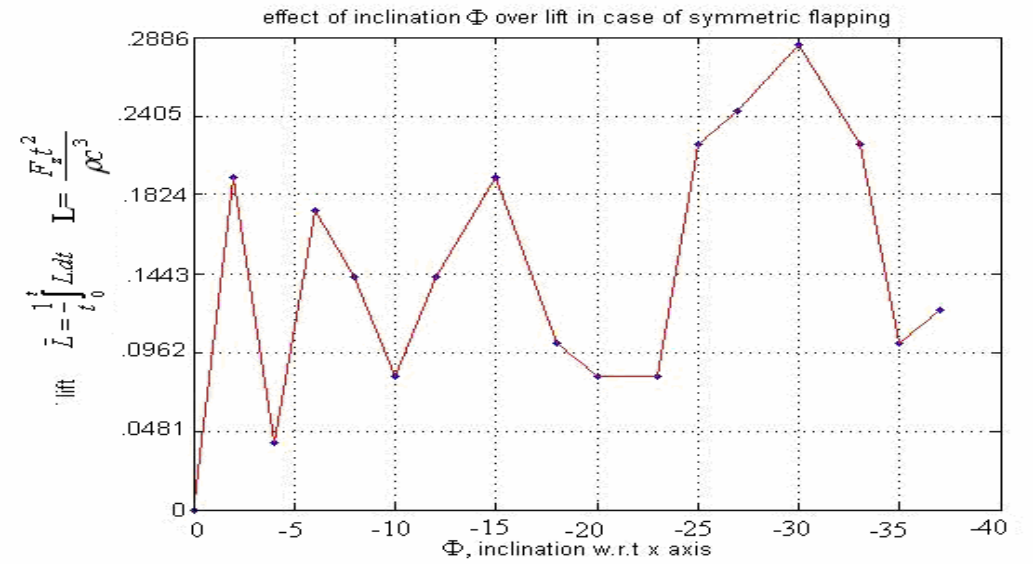

Fig 3.10 Effect of the inclination of the mean position wing on the lift .Wings are inclined at the given angles w.r.t horizontal axis

3.3.3 Asymmetric flapping

Unlike symmetric flapping asymmetric flapping is identified as lift generator even when the mean position of the wing is horizontal. As observed in nature, we have also maintained the downward stroke to be more faster than the upward stroke. Unlike symmetric flapping in this case most of the time only the 2 jets are formed which are moving in downward direction. The net downward momentum transfer by these jets in turn impart an upward thrust resulting in finite lift. In the following figures fig 3.11 the subsequent development of two jets will be observed in the velocity field of 1^{st}, 2^{nd}, 4^{th} and 20^{th} cycles. Figure 3.11 shows that in the 1^{st} cycle there are four jets in four direction but with 2^{nd} cycle the 2-directional jets sets in resulting in net lift. Fig. 3.12 shows the combined velocity and vorticity field of asymmetric flapping after 1^{st}, 3^{rd}, 11^{th}, 18^{th}, 20^{th} and 40^{th} cycles. The jets and the shedded vortices both are heading downwards.

Fig 3.13 presents the contour plot of the velocity field for asymmetric flapping. In all the figures of 3.13 it is evident that the high velocity zones and the shedded vortices are adjacent to wings. Fig 3.13a shows that during 1^{st} cycle the high velocity is very localized near the wings. Fig. 3.13 b, c, d suggests that the high velocity zone is spread for a wider area and the high velocity zone is moving in downward direction . So this downward momentum of fluid in turn imparts upward lift to wings. This also proves that the time averaged force becomes larger and larger with the number of flapping cycles till it attains a steady state value. Figure 3.14 shows the lift over 20 cycles of asymmetric flapping. Figure 3.15 shows that the non dimensional force as described in equation 3.3.1 in case of the asymmetric flapping is non zero. The negative of the time averaged force is the actual value of the lift.

3.3.4 Effect of inclination in asymmetric flapping

Figure 3.16 emphasizes the fact that with the increase of inclination of the mean position w.r.t horizontal axis lift increases. The mean inclination of the wing position helps in increasing do-

wnward component of the jets to enhance lift. Figures 3.17 a,b,c show the velocity field and vorticity field at the 20^{th} cycle of asymmetric flapping of different inclinations. Figure 3.17 d, e,f illustrates the velocity contours. It is evident that the jets of fig 3.17 a, d are confined within 0 to -1 of vertical axis whereas the jets in fig 3.17 c, f are rushing through the zone of -2 to -3. It proves that the downward component of the jet momentum is enhanced and hence causing the increase of lift.

3.3.5 Effect of angular amplitude

Figure 3.18 highlights the influence of angular amplitude on lift. The figure shows more or less an upward trend with the angular acceleration. Since the angular amplitude term directly appears in angular acceleration, the lift is increased. Unless the angular amplitude becomes so large that the wings interfere among themselves at the end of the downstroke, lift increases with the angular amplitude. Figure 3.19(a, c) and (b, d) shows the velocity contour & vorticity field at angular amplitudes of 80 degree and 135 degree with -20 degree initial inclination.

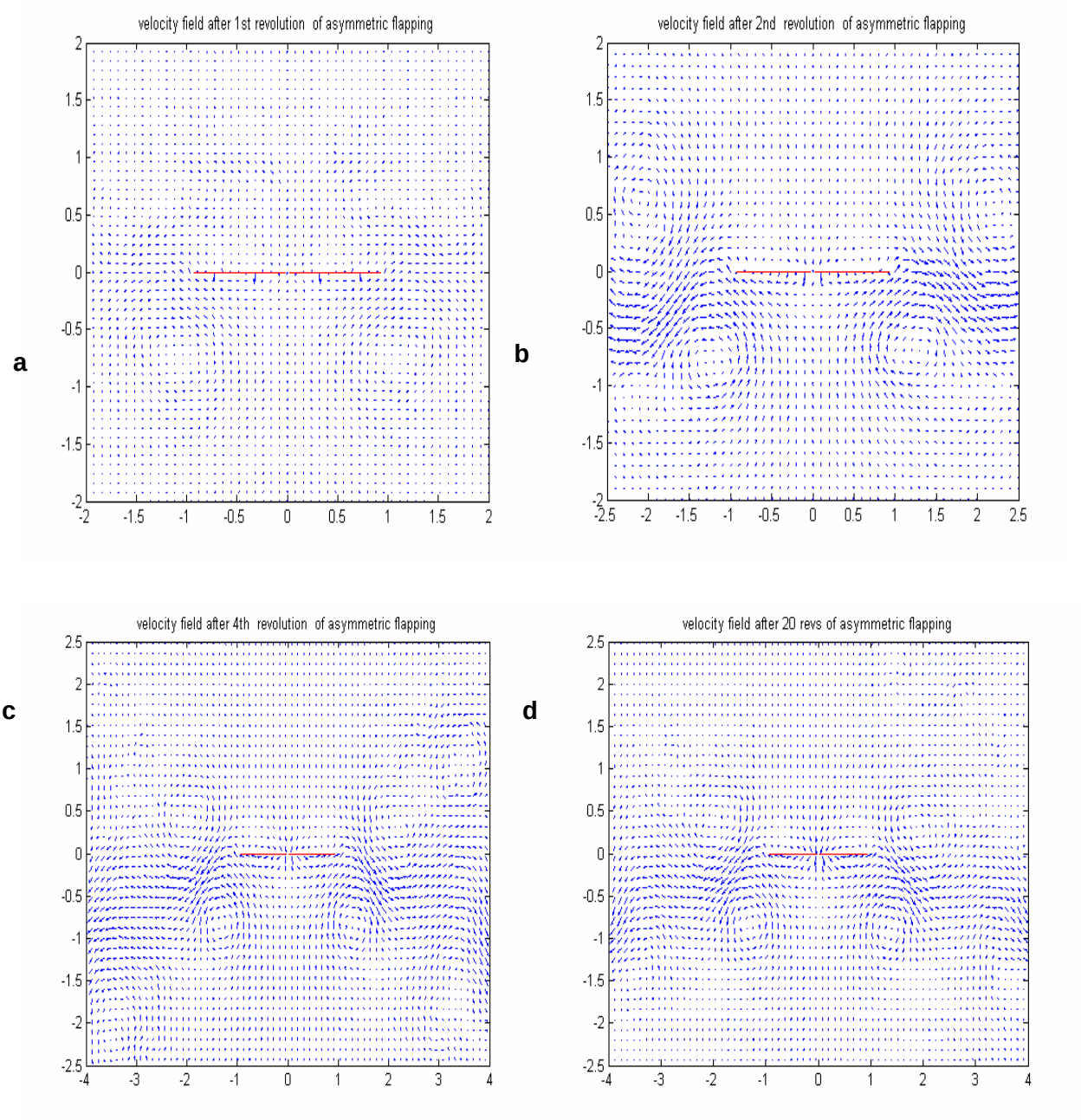

Fig 3.11 velocity field of asymmetric flapping with downstroke 30 rev/s and upstroke Speed: downstroke speed =1:2 (a) 1st revolution (b)2nd revolution (c) 4th revolution and (d) 20th revolution $\theta=80^o$; $\Phi=0^o$; $t_d=0.017$ sec; $t_u=0.034$ sec; AR=0.5;

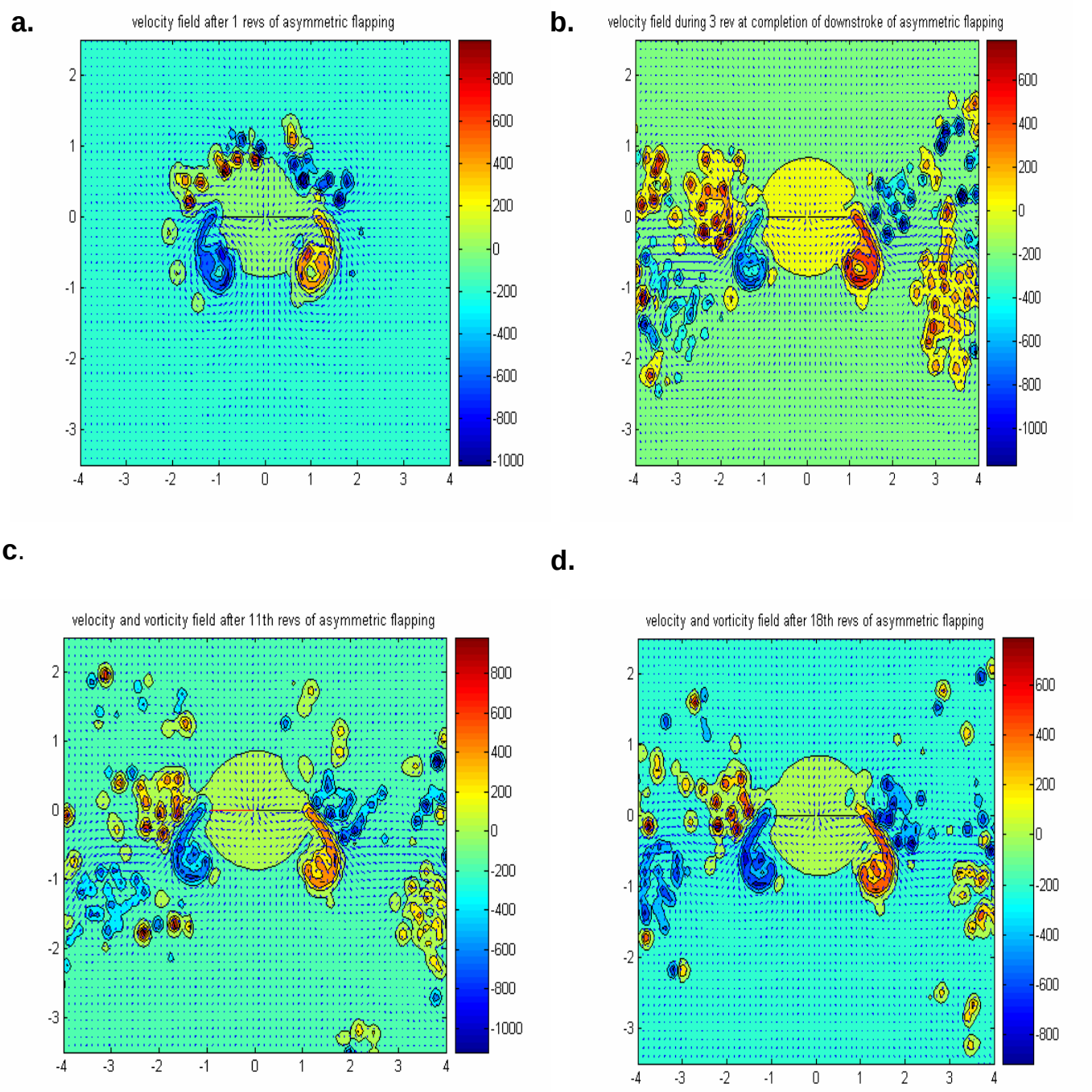

Fig 3.12 a) velocity and Vorticity field of 1st cycle (b) 3rd cycle
c) 11th cycle (d) 18th cycle
θ=80°; Φ=0°; t_d=0.017 sec; t_u=0.034 sec; AR=0.5;

e.

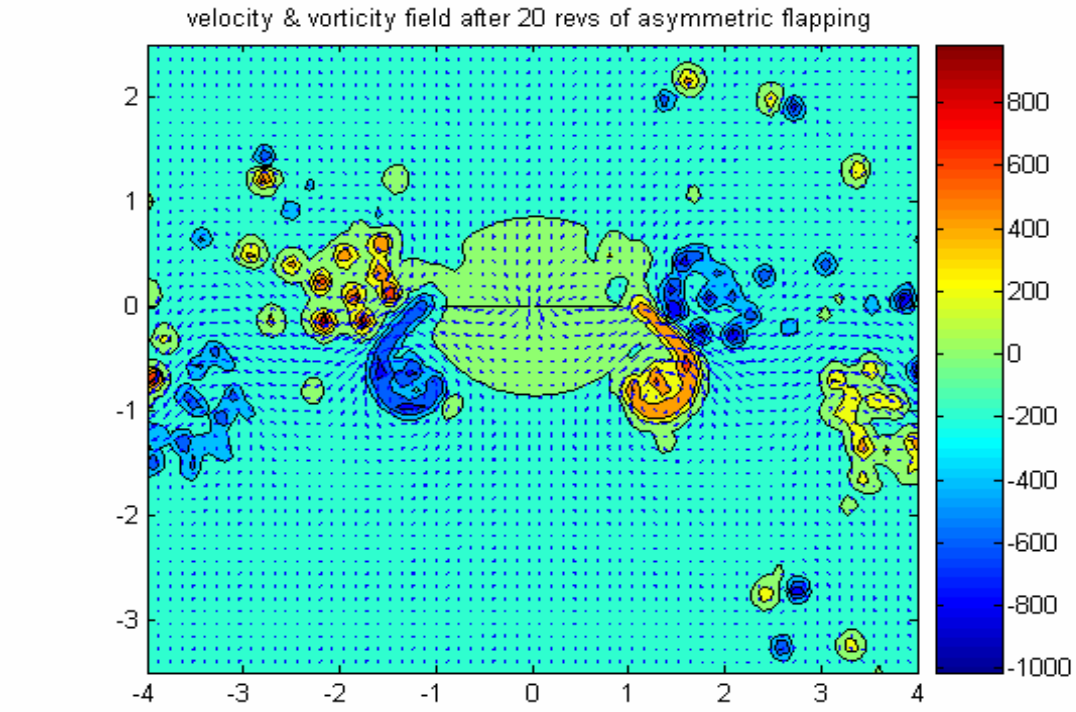

f.

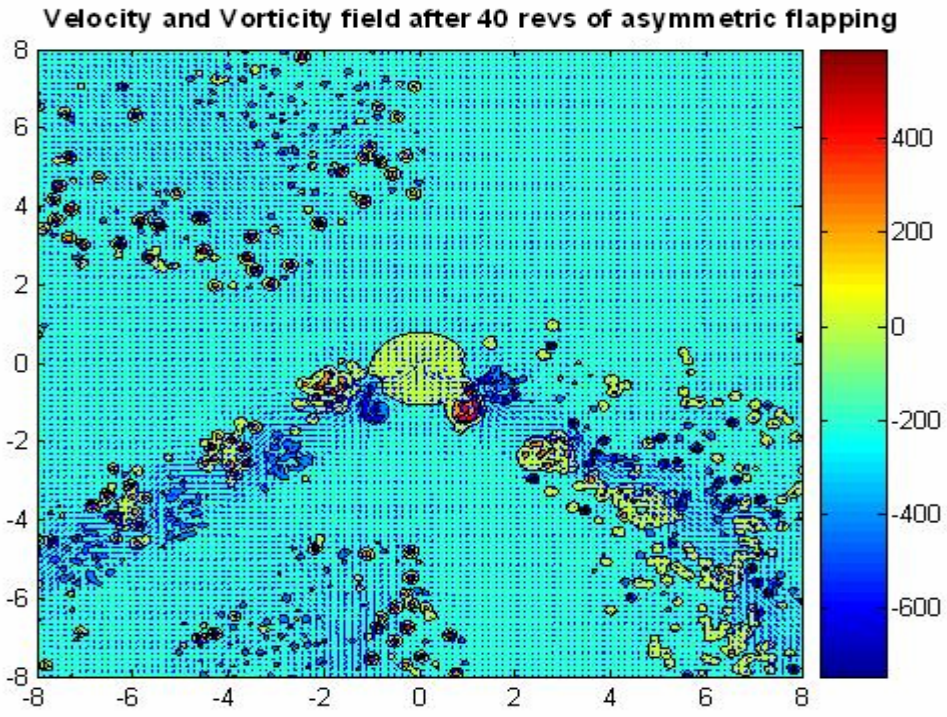

Fig 3.12 e) Velocity and Vorticity fields after 20 revs and f) 40 revs. $\theta=80^{o}$; $\Phi=0^{o}$; $t_d=0.017$ sec; $t_u=0.034$ sec; AR=0.5;

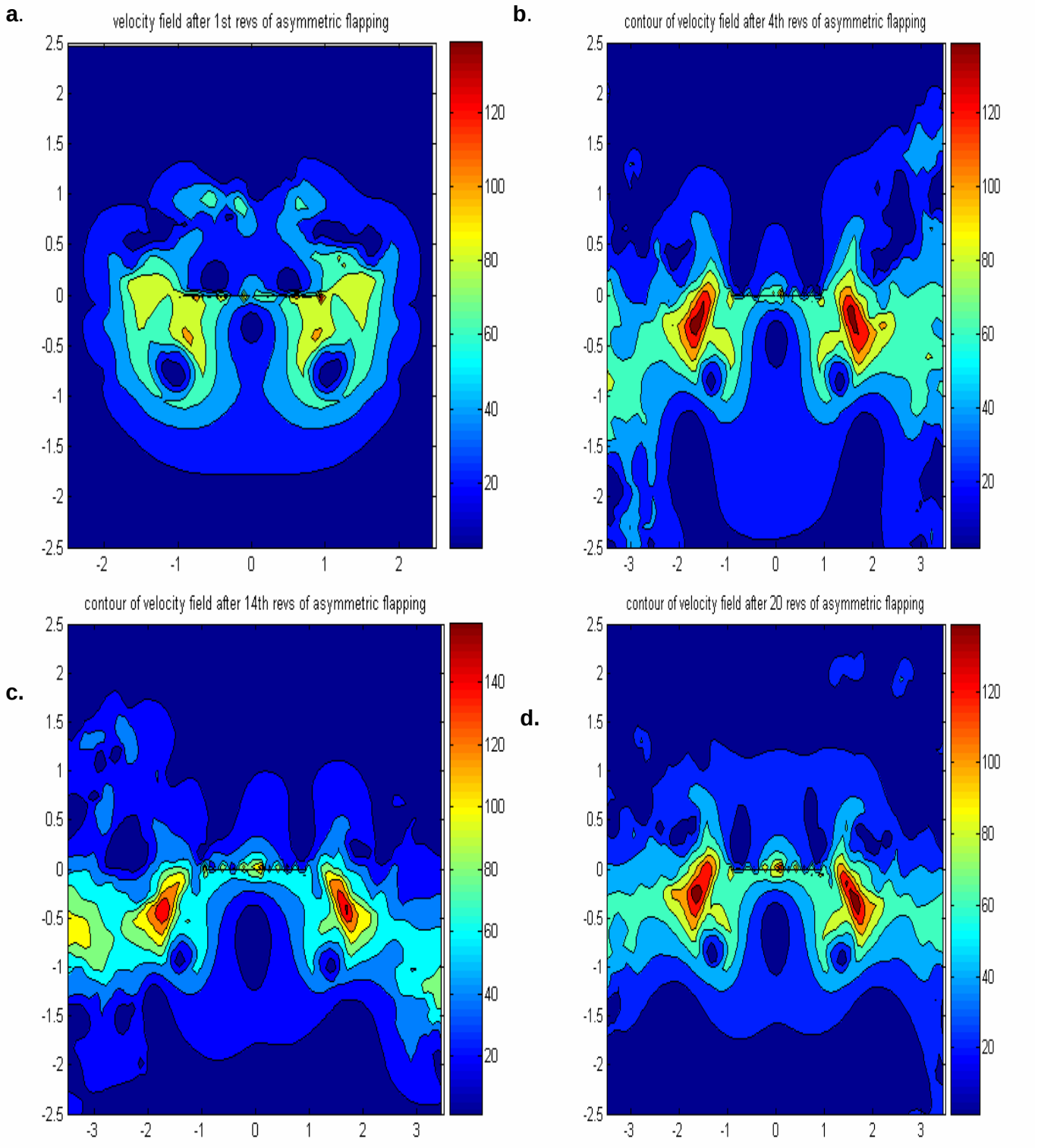

Fig 3.13 a) Velocity contour over the flow field in (a) 1st cycle (b) 4th cycle (c) 14th cycle (d) 20th cycle
θ=80°; Φ=0°; t_d=0.017 sec; t_u=0.034 sec; AR=0.5;

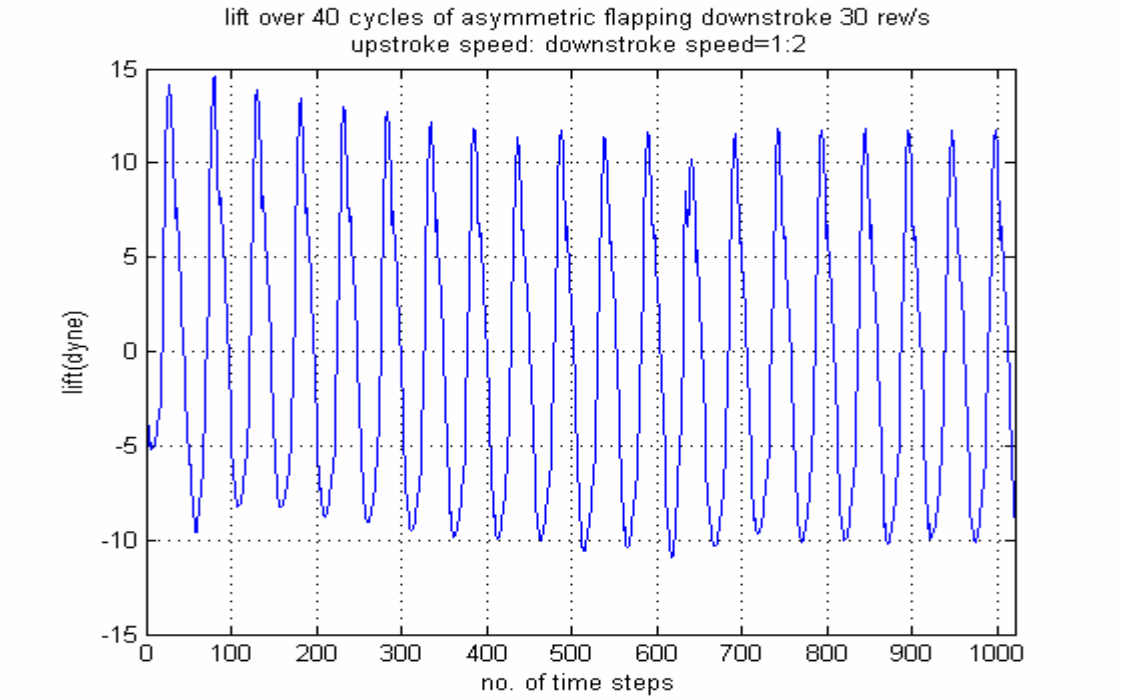

Fig 3.14 lift of asymmetric flapping for 20 cycles
$\theta=80^o$; $\Phi=0^o$; $t_d=0.017$ sec; $t_u=0.034$ sec; AR=0.5;

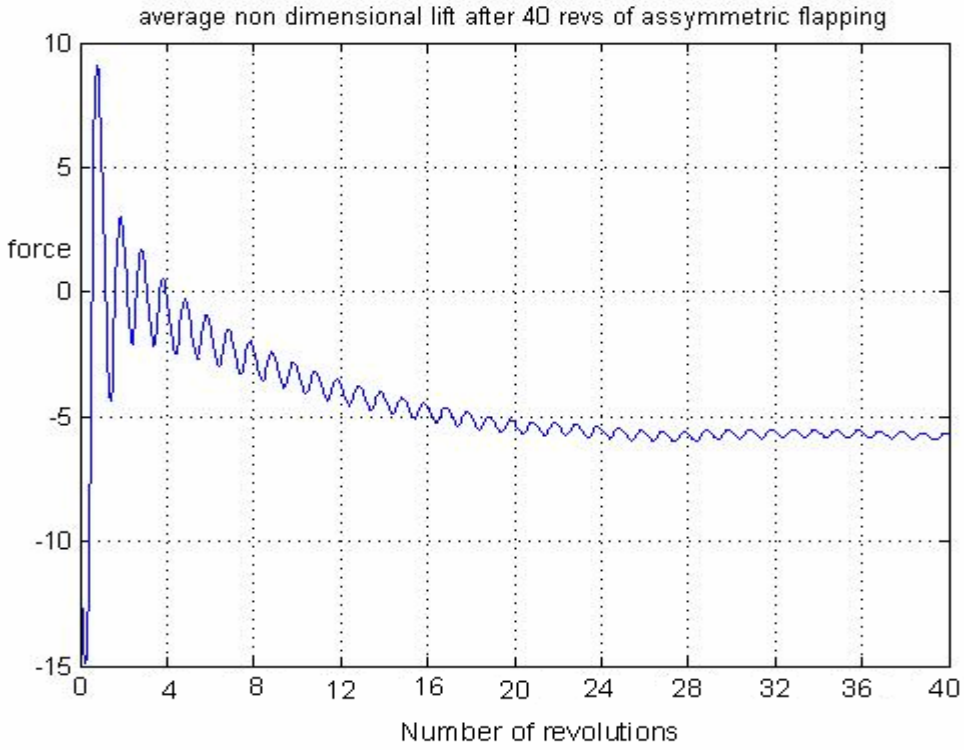

Fig 3.15 Average non dimensional lift over 40 revs of asymmetric flapping in case of rigid wings (upstroke speed=20 rev/s 80 degree amplitude) $\theta=80^o$; $\Phi=0^o$; $t_d=0.013$ sec; $t_u=0.026$ sec; AR=0.5;

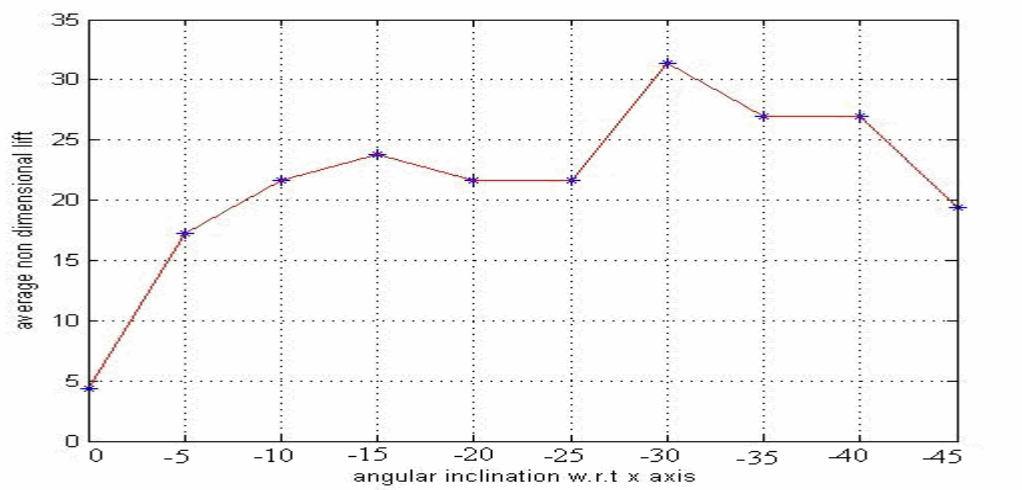

Fig 3.16 influence of angular amplitude on lift θ =80^o ; upstroke speed=20rev/s; upstroke speed:downstroke speed=1:2; t_d=0.013 sec; t_u=0.026 sec; AR=0.5;

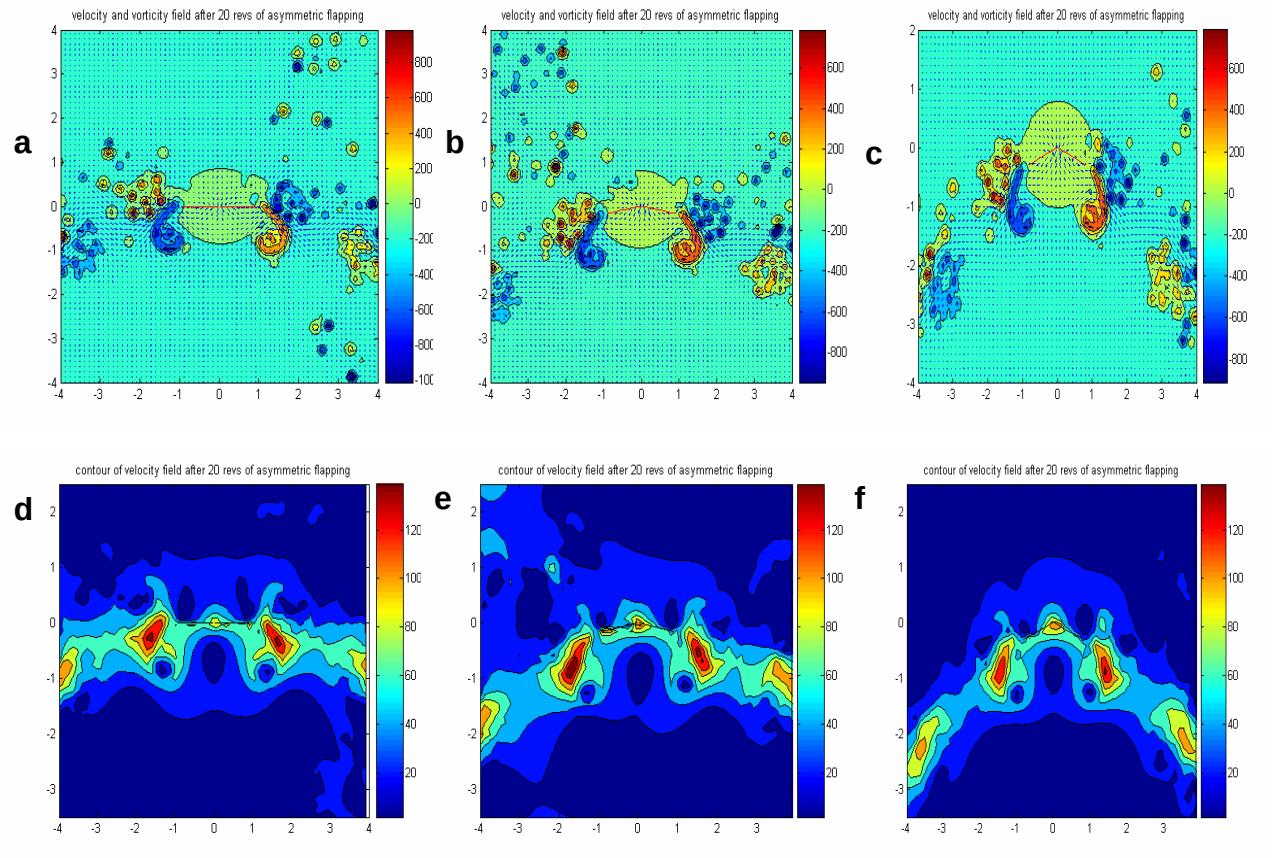

Figure 3.17 velocity and vorticity field at (a) Φ=0^o (b) Φ=-10^o (c) Φ=-20^o Contour of velocity field at (d) Φ= 0^o (e) Φ=-10^o (f) Φ=-20^o θ=80^o; t_d=0.013 sec; t_u=0.026 sec; AR=0.5;

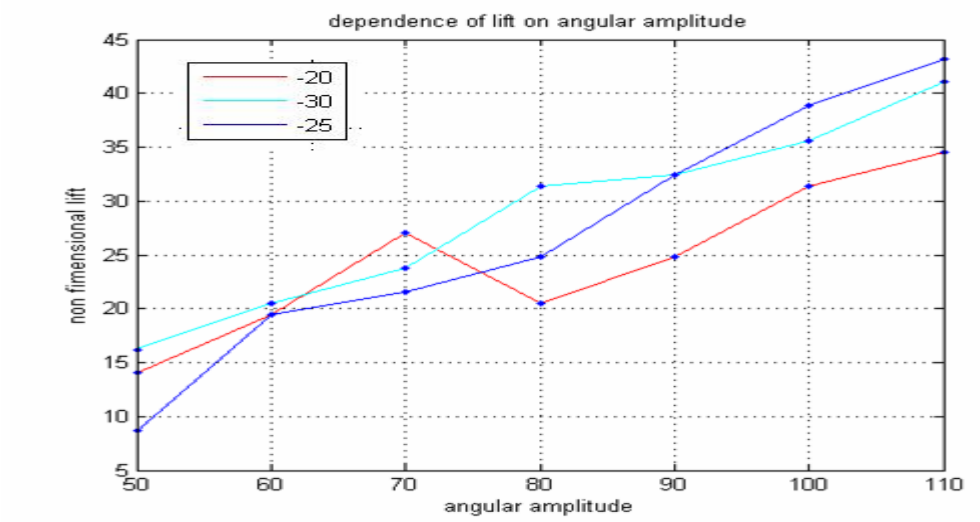

Fig 3.18 Influence of angular amplitude on lift with Φ=20^o, Φ=-25^o, Φ=-30^o; θ=80^o; t_d=0.013 sec; tu=0.026 sec; AR=0.5;

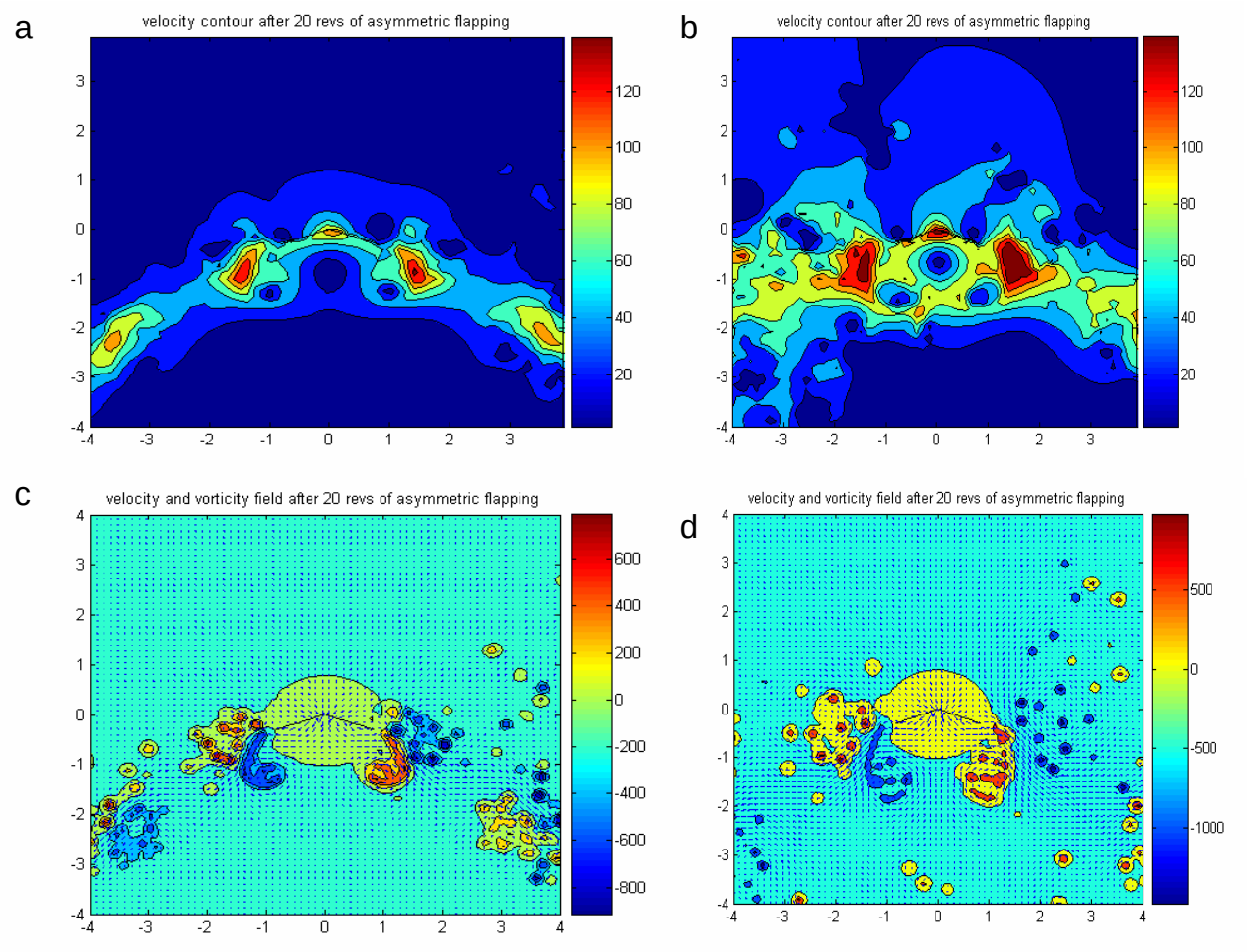

Figure 3.19 a) velocity contour at θ= 80^o b) at θ=135^o
c) vorticity and velocity field at θ=80^o d) at θ=135^o t_d=0.013 sec; t_u=0.026 sec; AR=0.5;

3.3.6 Effect of flexibility on lift

In this section the effect of flexibility of wings on lift performance is discussed. It is generally assumed that the wing deflection is determined by the combination of fluid dynamic pressure forces associated with flapping elastic processes of the wing. However the instantaneous curvature of the wings determines the spatial distribution of pressure stresses, thereby altering bending moments also. Thus coupling between fluid and solid loads is a pervasive and often an unresolved issue.

As there is uncertainty about the causes of the wing deformation, we have modeled each wing as cantilever beam and the loading is assumed to be proportional to the kinetic energy. Using proper boundary conditions, we calculate the deflection equation using the bending deflection equation. During the simulation, we assumed that the wing deforms during upstroke and remains rigid during downstroke. Figure 3.20 shows the different positions of the wing with deflected and rigid conditions.

$$E I \frac{d^4 y}{dx^4} = \frac{1}{2} \rho \omega^2 x^2$$ Bending deflection equation

Boundary conditions of the cantilever beam

$$1.\ E I \left.\frac{d^3 y}{dx^3}\right|_{x=0} = V_{x=0}$$

$$2.\ E I \left.\frac{d^2 y}{dx^2}\right|_{x=l} = -M_{x=l} = 0$$

$$3.\ \frac{dy}{dx} = 0 \quad \text{at } x = 0$$

$$4.\ y = 0 \quad \text{at } x = 0$$

The deflection equation is as follows:

$$EIy = \frac{\rho\omega^2 x^6}{720} - \frac{\rho\omega^2 l^3 x^3}{36} + \frac{\rho\omega^2 l^4 x^2}{16}$$

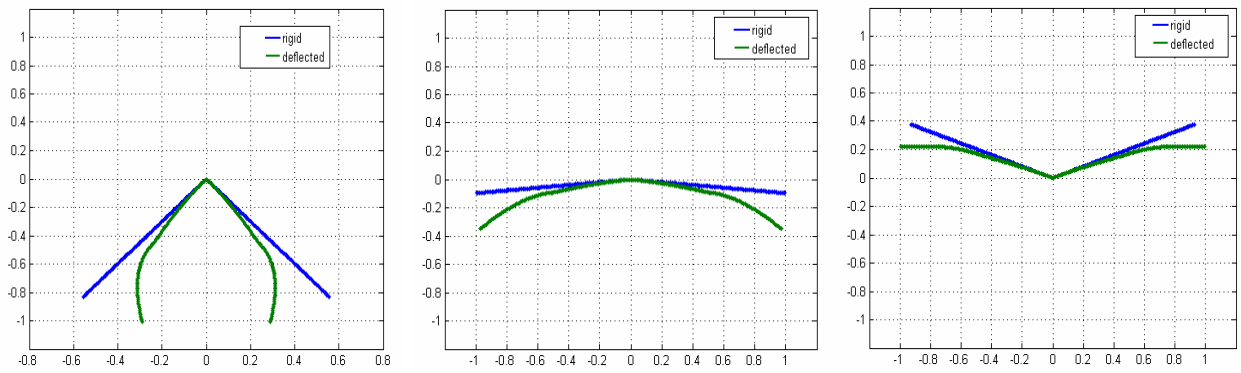

(a) **(b)** **(c)**

Figure 3.20 Rigid and deflected wing positions during upstroke at (a) -55^o (b) -5^o (c) 20^o with Φ=120^o and EI_{front} : EI_{rear} =5

Figure 3.21, 3.22 shows the influence of flexibility in case of symmetric flapping and asymmetric flapping respectively. On the asymmetric flapping the influence of flexibility is more prominent. Now considering $\frac{\rho\omega^2}{EI}$ as a parameter in the deflection equation we want to observe the effect of change of flexural stiffness EI. Keeping the 1st half of wing $\frac{\rho\omega^2}{EI}$ =1 and then reducing the other half's stiffness ,we want to find the optimum ratio for maximum lift generation.

Observing the figure 3.23a,b it can be said that $\frac{EI_{front}}{EI_{rear}}$ ratio ranging from 5 to 6 gives maximum lift.

3.3.7 Effect of asymmetry ratio

In this section the effect of upstroke speed to downstroke speed ratio is discussed. Figure 3.24 is the lift contour over asymmetry ratio (upstroke speed: downstroke speed ratio). Keeping each downstroke speed fixed we went on calculating lift for different asymmetric ratios ranging from 0.2 to 1 in steps of 0.05. It shows that lift increases with downstroke frequency. The optimum asymmetry ratio for maximum lift generation ranges from 0.4 to 0.7. Figure 3.25 shows the influence of asymmetry ratio for four downstroke speeds. Fig 3.26 shows that at lower speed the asymmetry ratio is around 0.4 to 0.55 and in higher speed it generally occurs near 0.7. Since the simulations have been done with asymmetry ratio at interval of 0.05 the error bar of ± 0.025 has been incorporated.

3.3.8 Effect of speed

Since calculation of lift involves the term $\rho U\Gamma$ and U inherently depends on angular frequency it's natural that lift increases with frequency. Figure3.27 shows lift Vs. Reynolds number where Reynolds number is based on average tip wing velocity and kinematic viscosity of air at 20^{o} C. However the nondimensional lift in figure 3.28 does not show clear trend.

3.3.9 Effect of size

Figure 3.29 shows the effect of size on lift .The contour plot reflects the fact that lifts increases with size as well as frequency. Figure 3.30 shows the comparison of lift calculated using vortex method and the formula given by Ellington(1999) .

The formula is as follows $: M = 0.387\frac{\Phi^2 n^2 R^4 C_l}{AR}$

where m(kg), Φ(rad), n(Hz) and R(m). Here C_L is assumed as 2 because 2-3 is generally ceffic-ient of lift for hovering(Ellington 1999). In our simulations we have initially calculated lift per unit depth of the plane. Then we calculate lift along the breadth. We have taken aspect ratio of wing to be 2. In Fig 3.30 a it is evident that lift is almost same in both the cases. With increase in wing length the dependence of fourth power on R given by Ellington's formula predicts, ho-wever our lift estimations are much smaller than the Ellington's formula. In fig 3.30 b, c the lift calculated by vortex method for the asymmetric flapping accounts 60% of Ellington's formula in 25-30 freq/s but beyond that it's much less.

3.3.10 Comparison using data on insects

a. **Small Fly**: It's frequency is 500 rev/s. Each wing length is about 5mm. Each wing breadth is taken to be 2.5 mm. Using zero degree inclination,150 degree amplitude and $\frac{t_d}{t_u}$ =0.5 our lift is 219.26 dynes. Ellington's formula gives us mass=207.22 mg. As one gm weight=981 dynes the force is equal to 203.28 dynes.

b. **Mosquito:** It's frequency ranges from 150 Hz to 300 Hz. Using upstroke frequency =150 Hz.

and downstroke speed=300 rev/s the effective frequency is 200 Hz .Each wing length and breadth is taken to be 8mm and 4mm respectively. Mosquito weight is 3mg .Using 170 degree of angular amplitude our calculation is 159.31 dyne. Ellington's formula yields 273.79 dyne. Both the calculations indicate the lift generated is much higher than that needed for sustaining its weight (3mg-wt=2.943dyne). It's our speculation that due to very small sizes it experiences substantial drag which is not accounted in our inviscid calculation.

c. Butterfly: It's frequency is 20 Hz, using 5cm wing length, mean breadth 5cm, 80 degree of angular amplitude, $\frac{t_d}{t_u}$ =0.5 and our calculation gives 1706.5 dyne. Ellington's formula gives 1.9gram or 1863.9 dyne. Using data from SanDiego zoo site butterfly wing ranges from 0.3cm to 30 cm with body weight ranging from 0.003 grams to 3 grams. If for 5cm wing span the body weight is about 1-1.5gm, again this is less than both our calculations and Ellington's estimation.

$$L_{av} = \frac{1}{t}\int_0^t L\,.dt \qquad \bar{F} = \frac{L * (t_d + t_u)^2}{\rho C^3}$$

Average non dimensional lift over 20 revs of symmetric flapping 20revs/sec 80 degree of amplitude for rigid wing

Average non dimensional lift over 50 revs of symmetric flapping 20 rev/s 80 degree amplitude for flexible wing

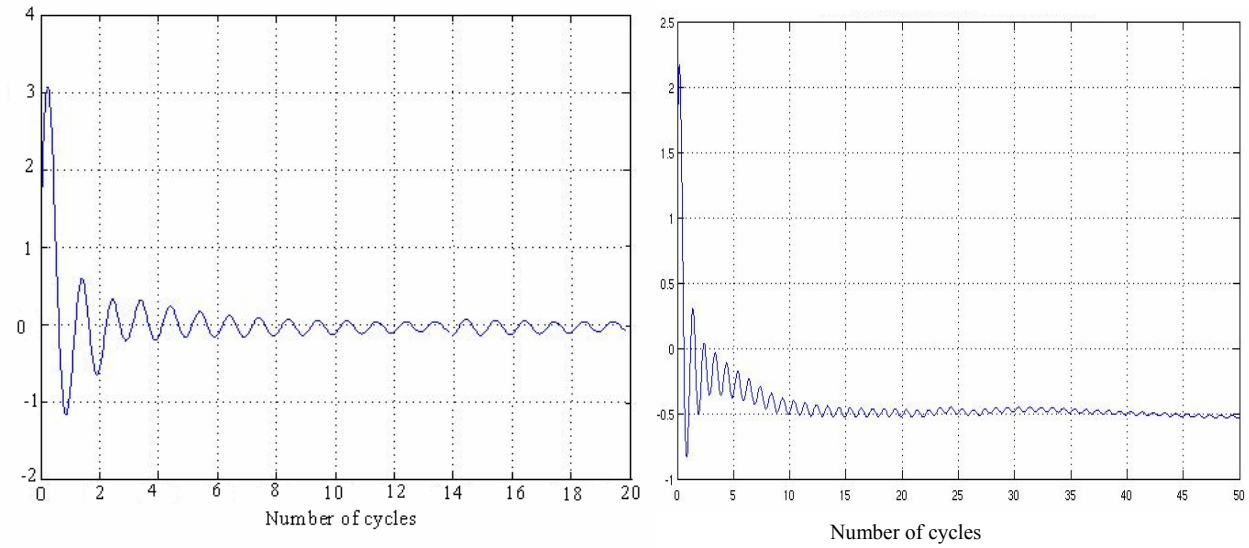

Figure 3.21 influence of flexibility in case of symmetric flapping θ=80°; t_d=0.025 sec; t_u=0.025 sec; AR=1;Φ=0

Average non dimensional lift over 40 revs of asymmetric flapping in case of rigid wings (upstroke speed=20 rev/s 80 degree amplitude)

Average non dimensional lift over 40 revs of asymmetric flapping in case of flexible wings (upstroke speed=20 rev/s 80 degree amplitude)

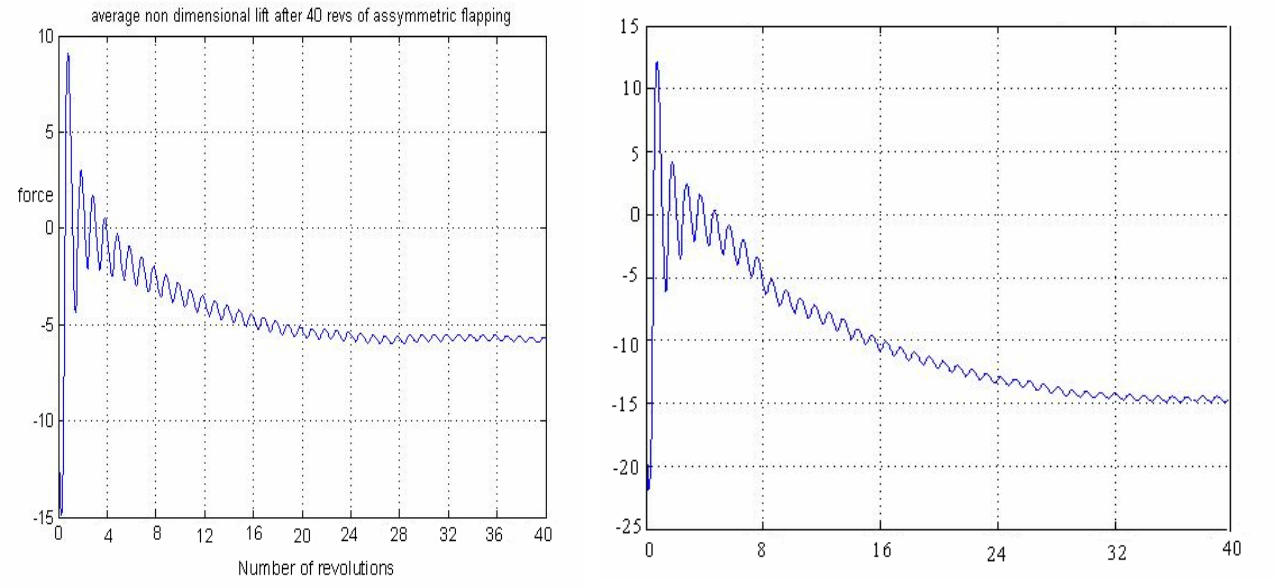

Figure 3.22 influence of flexibility in case of asymmetric flapping θ=80°; t_d=0.013 sec; t_u=0.026 sec; AR=0.5; Φ=0

a **b**

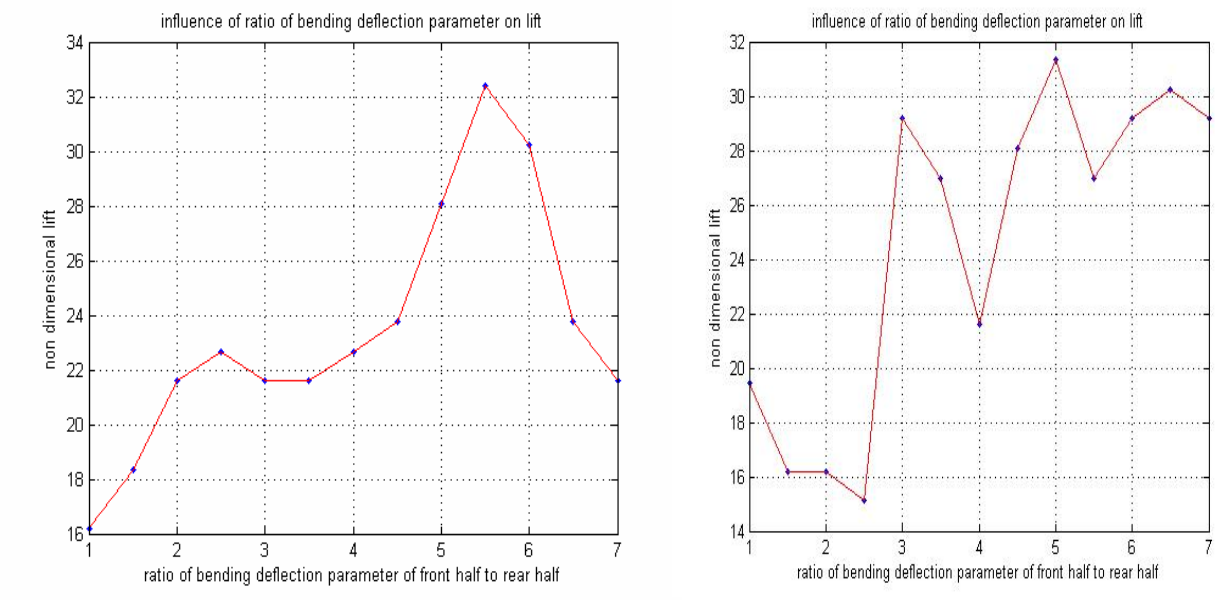

Φ=-25°; θ=80° **θ=80°; Φ= -30°**

Fig 3.23 Influence of bending deflection parameter ratio on lift t_d=0.013 sec; t_u=0.026 sec; AR=0.5;

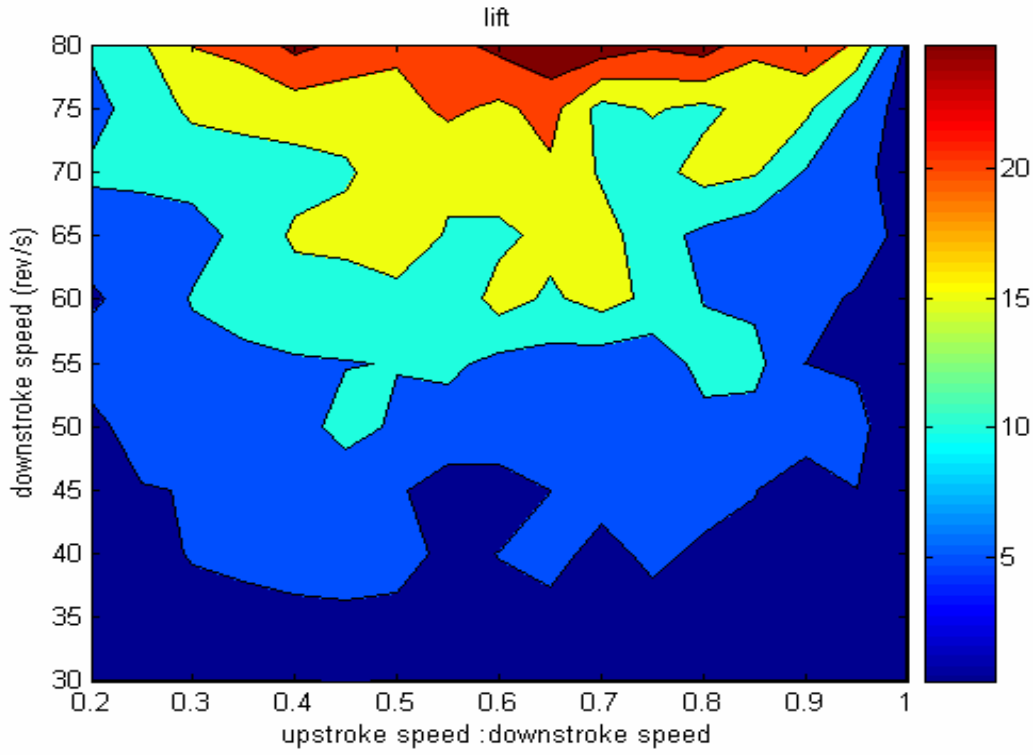

Fig 3.24 lift contour plot with downstroke frequency and asymmetry ratio.Φ= -25°; θ=80°; for a fixed downstroke speed upstroke speeds are varied and thus asymmetry ratio is varied.

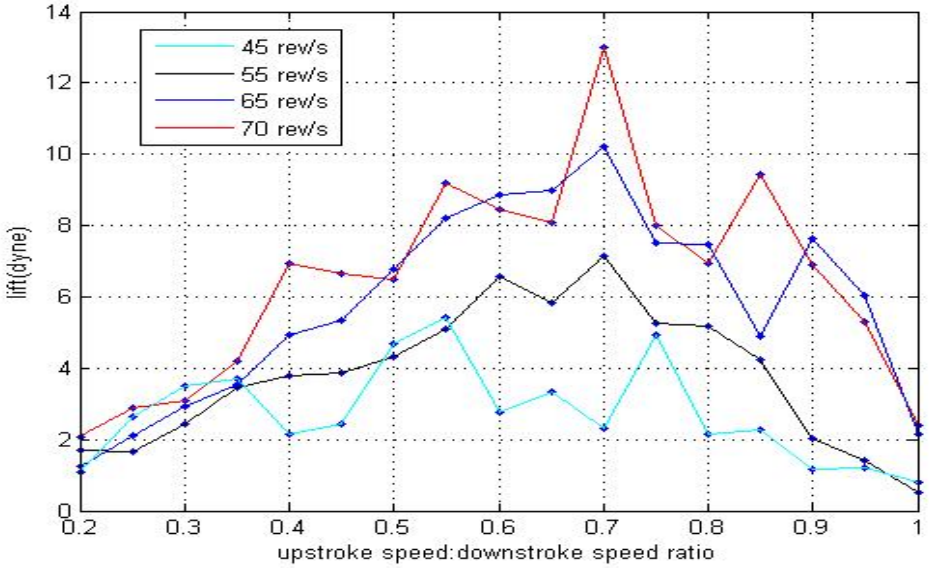

Figure 3.25 Lift vs. asymmetry ratio Φ= -20°; θ=80°;

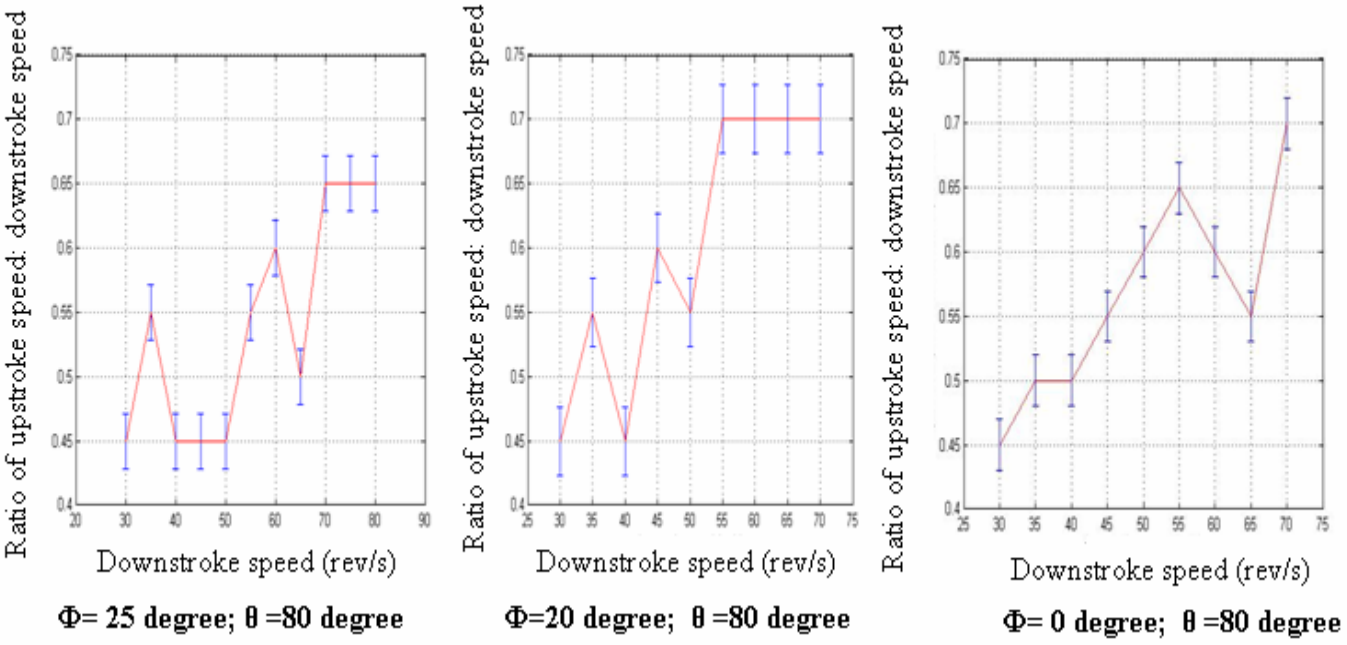

Figure 3.26 Ratio of upstroke speed: downstroke speed at which highest lift occurs Vs. Downstroke speed

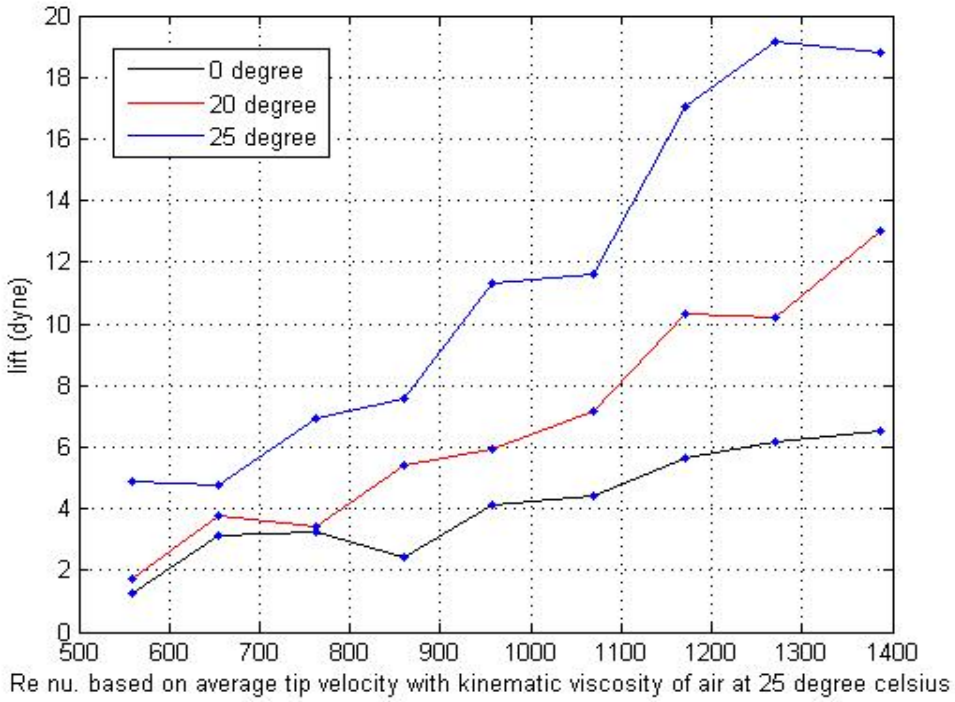

Figure 3.27 Lift vs. Reynolds number Φ=0°,-20°,-25°, θ=80°; The AR at which highest Lift occurs for a fixed downstroke speed is selected .

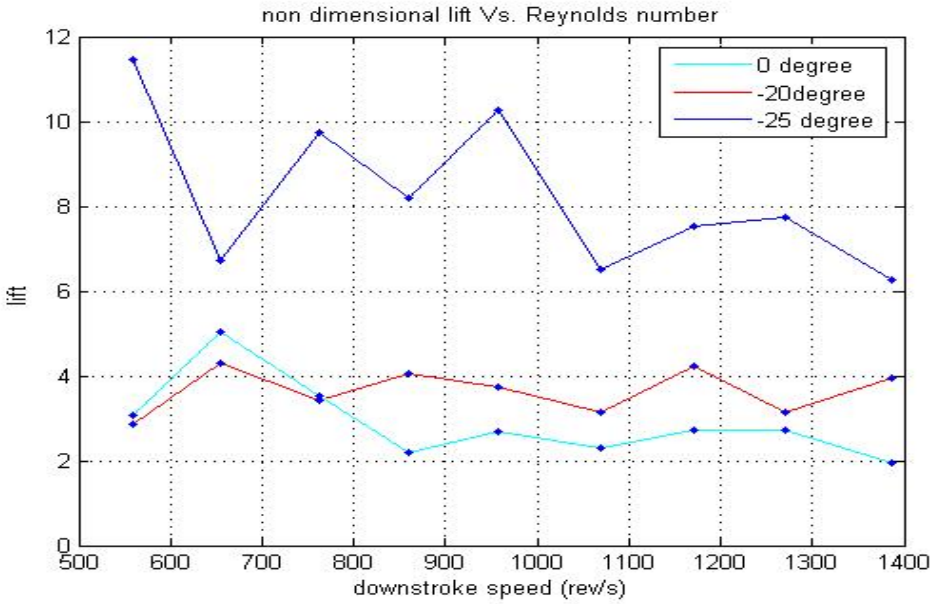

Figure 3.28 Non dimensional Lift Vs. Reynolds Number Φ=0°,-20°,-25°; θ=80°; The AR at which highest Lift occurs for a fixed downstroke speed is selected

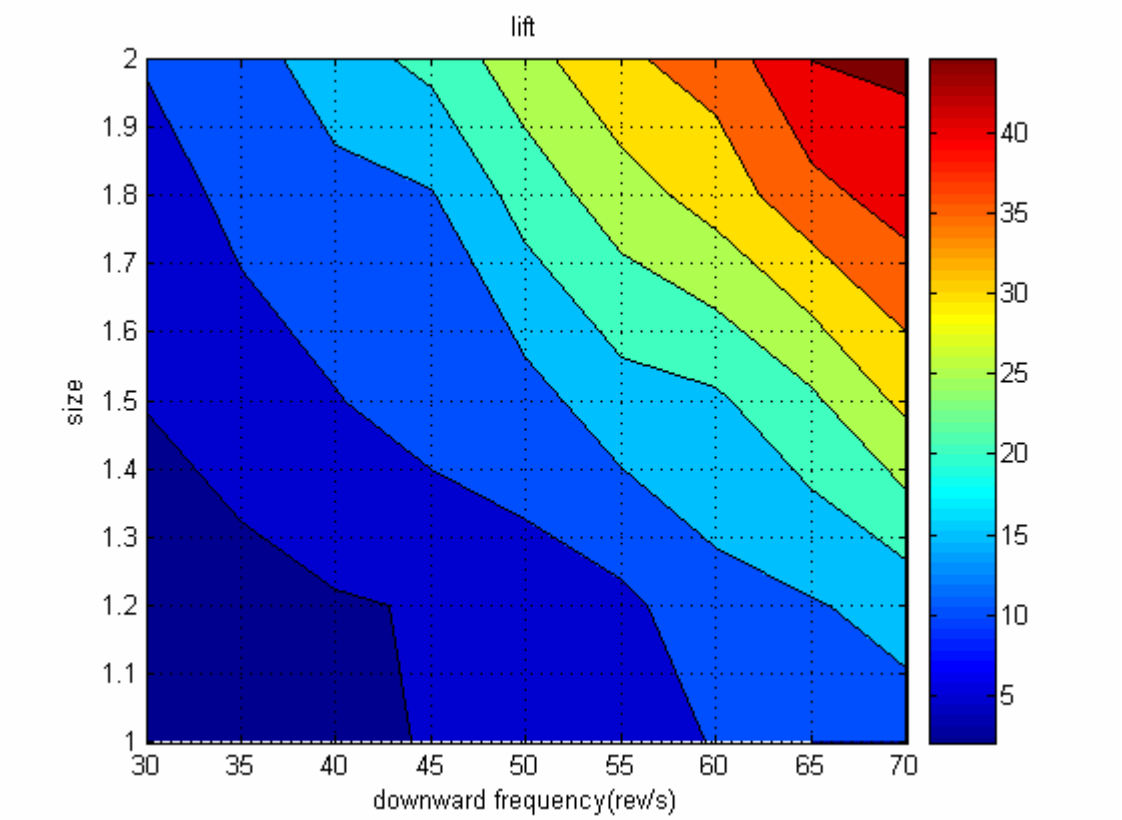

Fig 3.29 Contour of lift (dynes) over size (cm) and downstroke frequency (rev/s). $\Phi=-25^{o}$, $\theta=80^{o}$; The AR at which highest Lift occurs for a fixed downstroke speed is selected

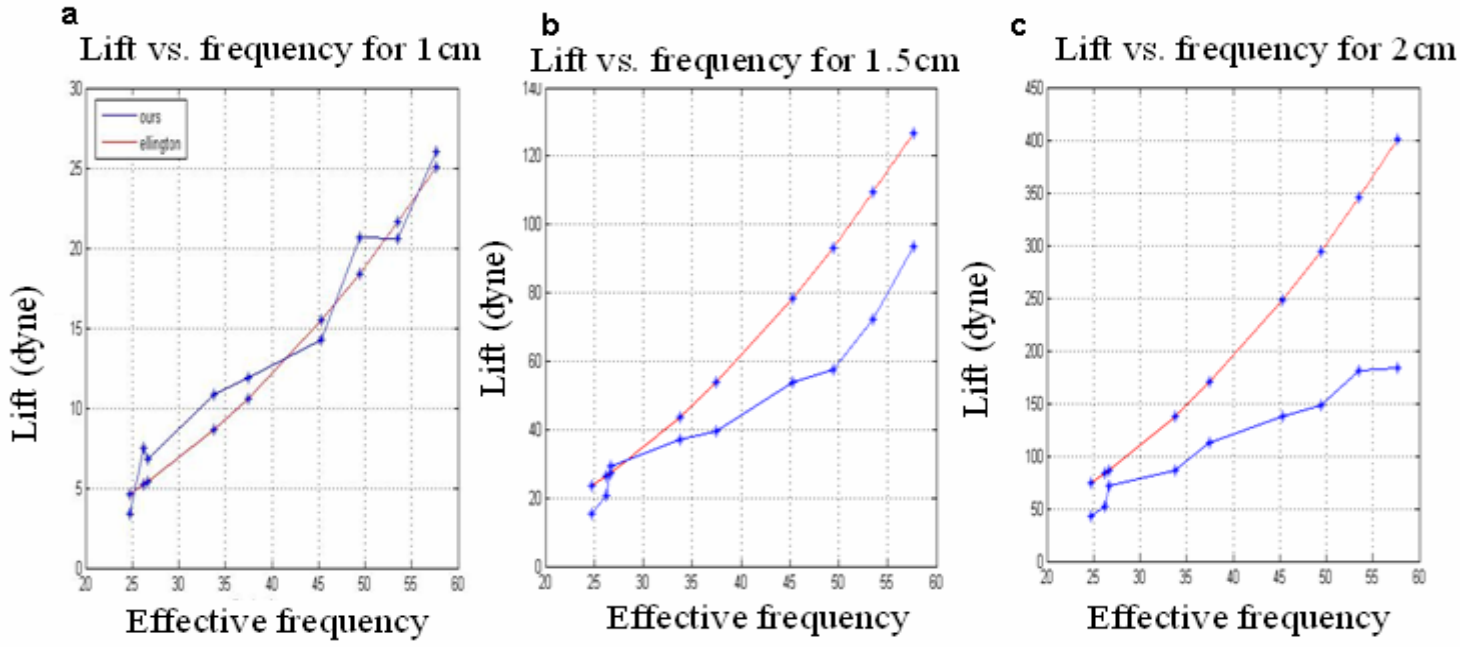

Fig 3.30 Comparison of lift calculates using vortex method and Ellington's formula a) 1cm b) 1.5 cm c) 2cm $\Phi=-25^{o}$; $\theta=80^{o}$; The AR at which highest Lift occurs for a fixed downstroke speed is selected

Chapter 4
CONCLUSION

In this chapter the conclusions are summarized based on our experimental and simulation results conducted on flapping wings.

1. Flow visualization figures obtained by the experiments on mechanical flapping models suggest that due to momentum transfer in both upward and downward directions, net lift produced in symmetric flapping is zero. On the other hand momentum is transferred in the downward direction in case of asymmetric flapping which yields a net upward lift to the wings. Also velocity fields obtained by numerical simulation of flapping wings supports the conclusion drawn from experimental observations.

2. For the mean position of the wings aligned with the horizontal axis the net lift produced over a cycle is nearly zero. If the mean position of the wings is inclined to the horizontal axis i.e. $\Phi \neq 0$, lift is generated even in the case of symmetric flapping although the lift is small. Generally with the increase of inclination (Φ) lift increases. In case of asymmetric flapping lift is substantially enhanced.

3. Lift increases with the angular amplitude. However amplitude θ must not be such that the flow between the wings interact with each other at the end of downstroke or upstrokees to hamper the lift generation.

4. In order to mimic the flexible wings we have examined the impact of flexibility of wings on lift. As we don't have clear idea regarding loading and EI of the wings, we have imposed loading on the wings and created deflection on wings. When flexibility is imposed along the wing length during upstroke, lift is increased.

5. From our experiments and simulations it's evident that asymmetry in upstroke speed

and downstroke speed generates positive lift. So we examined the optimum range of asymmetry ratio for maximum lift. The asymmetry ratio (upstroke speed:downstroke speed) should be around 0.4 to 0.5 for frequency upto 45 rev/s and 0.6-0.7 for higher wing beat frequency (45-70 rev/s) to generate optimum lift. However, experimental verification is essential.

6. Simulation using vortex method and with asymmetric flapping, we could account almost full lift for 1cm wing in comparison with Ellington's formula (1999). Ellington has considered coefficient of lift around 2. Our lift is equal to lift estimated by Ellington formula in the case of chord length 1cm and accounts nearly 60% in case of larger wing sizes like1.5cm and 2cm. In spite of not considering various viscous mechanism like delayed stall, leading edge separation bubble, we could account large fraction of the lift by asymmetric flapping. So it can be claimed that the asymmetry flapping is an effective & important way of producing lift.

In spite of our simulations we feel that experimental evidence is essential for verifying our simulation results. Particle image velocimetry (PIV) of the flow field can be an effective tool in matching the vorticity and velocity field generated by simulation. High speed photography of hovering insects is also an effective way of detecting the asymmetry in insect flights. Force measurement in mechanical flapping models with the help of quality sensors can also give a clearer picture of the lift profiles and utility of asymmetric flapping and wing flexibility.

APPENDIX-I

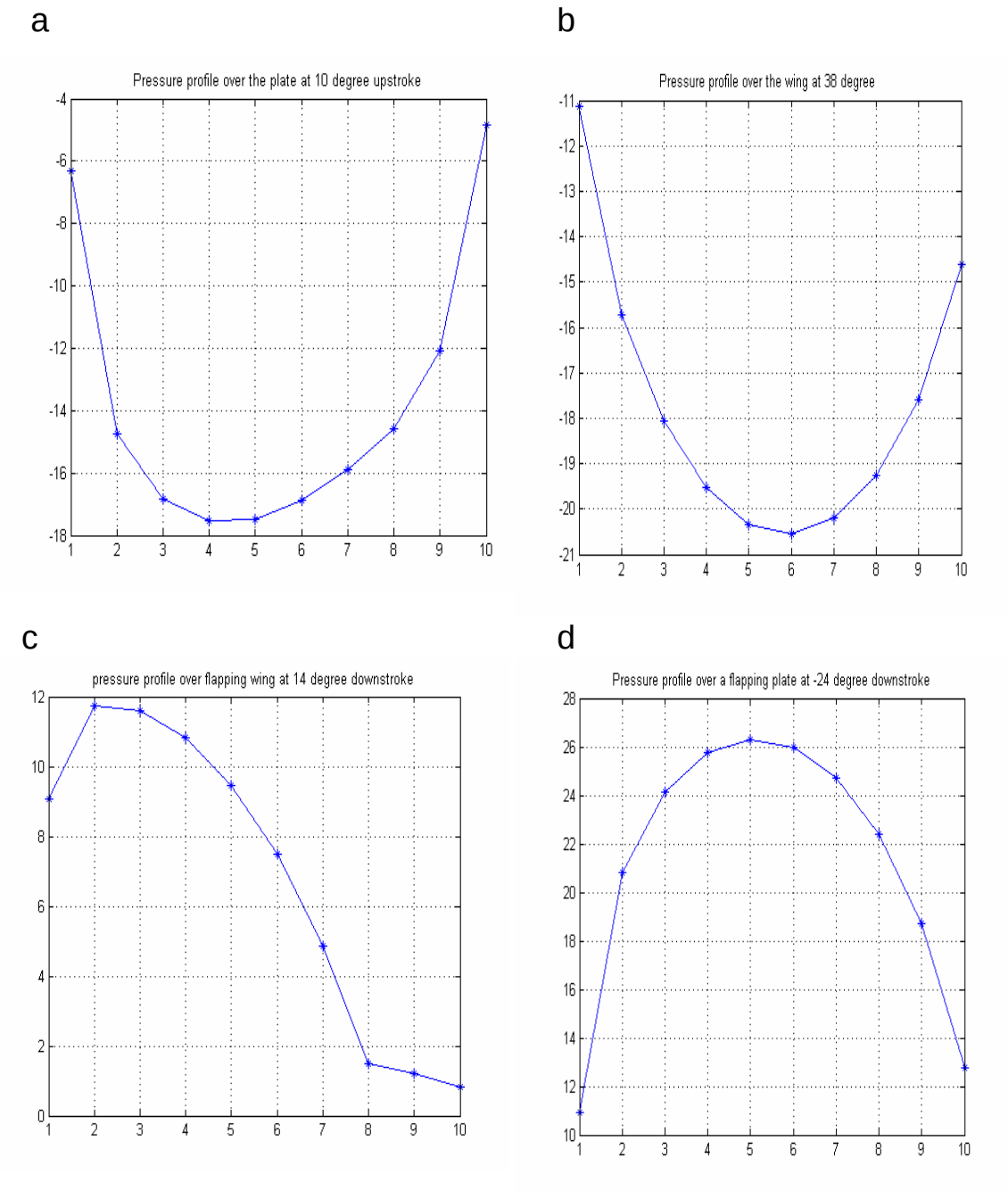

Fig 5.1 Pressure distribution over a flapping wing at (a) 10^o upstroke (b) 38^o upstroke (c) at 14^o downstroke (d) -24^o downstroke ; $\theta=80^o$; $\Phi=0^o$; $t_u=t_d=0.025$ sec

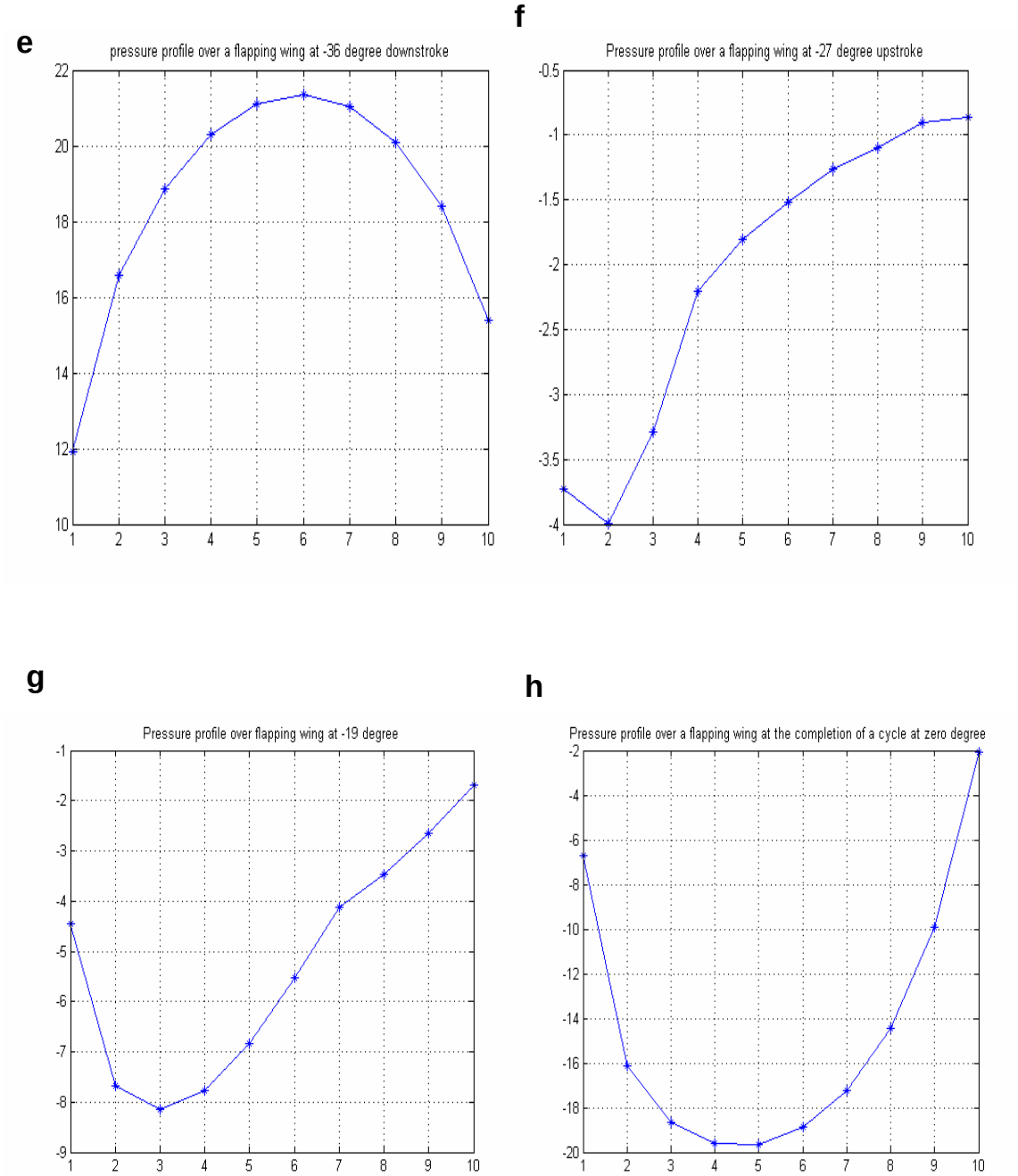

Fig 5.1 Pressure distribution over a flapping wing at (e)-36^o downstroke (f) -27^o upstroke (g) at 14^o upstroke (h) -24^o upstroke $\theta=80^o$; $\Phi=0^o$; $t_u=t_d=0.025$ sec

Bibliography

Bennet, L. 1977 Clap and fling aerodynamics-an experimental evaluation. J. exp. Biol. 69,261-272

De Laurier JD, Harris JM, 1982 Experimental study of oscillating wing propulsion J. Aircraft 9:368-73

De Laurier JD, Mueller TJ 2003 Aerodynamics of Small Vehicles Annu. Rev. Of fluid Mechanics 35:89-111

Dickinson, M.H., Lehman, F.O. and Sane S. P. 1999 Wing Rotation and the aerodynamic basis of insect flight. Science 284, 1954-1960

Dickinson, M.H. and Gotz, K.G.1993 Unsteady aerodynamic performance of model wings at low Reynolds number J. Exp. Biol. 174, 45-64

Dickinson, M.H.1994 The effects of wing rotation on unsteady aerodynamic performance at low Reynolds number. J. exp. Biol. 192 179-206

Dudley, R. 1991 Biomechanics of flight in Neotropical butterflies aerodynamics and mechanical power requirements. J. exp. biol. 192, 179-206

Ellington C.P, Unwin DM 1979 An optical tachometer for measurement of wing beat frequency J. exp. Biol. 82,(1):379

Ellington C.P, C van den Berg 1997 The Vortex wake of a "Hovering" Model Hawkmoth Phil.Trans. of Royal Soc. Lond. B 183 217-248

Ellington C.P 1999 The novel aerodynamics of insect flight: applications to micro air vehicles Journal of experimental Biology 202, 3439-3448

Ellington C. P. 1984 a The aerodynamics of hovering insect flight I: Quasi steady analysis Phil. Trans. R. Soc. Lond. B 305, 1-15

Ellington C.P. 1984 b The aerodynamics of hovering insect flight II: Morphological Parameters, Phil. Trans. R. Soc. Lond. B 305, 17-40

Ennos, AR 1989 Inertial and aerodynamic torques on the wings of Diptera flight J. Exp. Biol. 142,87-95

Jensen, M 1956 Biology and Physics of locus flight 3, The aerodynamics of locus flight Phil. Trans. R.Soc. Lond. B 239, 511-552

Ennos, A.R 1989 Inertial and aerodynamic torques on the wings of diptera in flight J. Exp. Biol. 142, 87-95

Hamdani, H. and Sun, M. 2000 Aerodynamic forces and flow structures of an airfoil in some

unsteady motions at small Reynolds number. Acta Mechanica 145,173-187

Katz J, Plotkin A Low speed aerodynamics Cambridge University press

Katz J, and Weihs D, Behaviour of vortex wakes from oscillating airfoils J.Aircraft Vol 15, No. 12,1978

Kellog J, Bovais C, Cylinder D, Dahlburg J, Foch R et al 2001 b Non conventional aerodynamics for MAVs. Proc. Int. Conf. Unmanned Air Veh. System 16th, Bristol, UK pp 26 1-12 Bristol, UK: Univ. Bristol

Kramer, M. 1932 Die Zunahme des Maximalauftriebes von Tragflugeln bei plotzlicher Anstellwinkelvergrosserung (Boeneffekt). Z. Flugtech. Motorluftschiff . 23 185-189

Lighthill, MJ 1973 On the Weis-Fogh mechanism of lift generation, J. Fl. Mech 60;1-17

Lissaman PBS 1983 Low Reynolds number airfoils Annu. Rev. Fluid Mech. 15:223-39

Maxworthy, T. 1979 experiments on the Weis-Fogh mechanism of lift generation by insects in hovering flight . Part 1. Dynamics of the 'fling'. J Fluid Mech. 93, 47-63

McMaster JH, Henderson ML 1980 Low speed single element airfoil synthesis Tech. Soar. 6:1-21

Mueller TJ 1985 Low Reynolds number vehicles In Advisory Group for Aerospace Research and Development AGARD-AG-288 ,ed. E Reshotko. Essex: Spec. Print. Serv. Ltd. 69 pp

Polhamus, E. 1971 Predictions of vortex lift characteristics by a leading edge suction analogy J. Aircraft 8,193-199

Ramamurti, R. and Sandberg, W.C. 2002 A three dimensional computational study of the-aerodynamic mechanisms of insect flight J. Exp. Biol. 205, 1507-1518

Sanjay P. Sane 2003 The aerodynamics of insect flight, journal of experimental biology 6, 4191-4208

Sane, S.P. and Dickinson M.H. (2002) The aerodynamic effects of wing rotation and a revised quasi-steady model of flapping flight. J. exp. Biol. 205, 1087-1096

Spedding, G.R. and Maxworthy, T. 1986 The generation of circulation and lift in a rigid 2-dimensional fling J. Fluid Mech. 165, 247-272

Sreyash J.V. 2005 MS thesis, JNCASR India: Experimental and numerical study of flapping wing flight

Thomas J. Mueller and James D. Delaurier 2003 aerodynamics of Small Vehicles Annual Review of fluid Mechanics 35:89-111

Vogel, S.1994 Life in Moving Fluids: he physical biology of flow. Princeton University P-ress

Walker, P.B. 1931 Experiments on the growth of circulation about a wing and an apparatus for measuring fluid motion, Rep.Memo. Aeronaut. Res. (Great Britain) No 1402

Walker, J 2002 Rotational lift: something different or more of the same? J. Exp. Boil. 205, 3783 -3792

Wang Z.J. 2000 two dimensional mechanism for insect hovering .Phys. Rev. Lett. 85, 2216-2219

Weis Fogh,T 1973 Quick estimates of flight fitness in hovering animals, Including Novel mechanisms for lift production J.Exp. Biol. 59,169-230

Wu J 1981 Theory for aerodynamic force and moment in viscous flows AIAA Journal 19,43 2-441l

Zanker, J.M and Gotz K.G 1990 The wing beat of drosphila melanogaster 2. Dynamics, Phil. Trans. R.Soc. Lond. B327 19-44.

Usherwood, J.R and Ellington, C.P (2002b0 The aerodynamics of revolving wings 2 Prope-ller force coefficients from mayfly to quail J. Exp. Biol. 205,1565-1576